Mourad Mohamed Mansour Gad Mohamed

Grid Code Compliance Testing Using Simulation

School of Technology and Innovations

Master of Science in Technology

Master’s thesis in Electrical Engineering

Vaasa 2026

UNIVERSITY OF VAASA
School of innovation Technology
Author: Mourad Mohamed Mansour Gad Mohamed
Thesis title: Grid Code Compliance Testing Using Simulation
Degree: Master of Science in Technology
Supervisor: Mustafa Alrayah Hassan Ibraheem
Instructor: Shahin Fouladi Panah
Partner Supervisor: Muhammad Khurram Shahzad
Year of graduation: 2026 **Number of pages:** 99

ABSTRACT:
The accelerating integration of inverter-based resources (IBRs) into power systems has fundamentally transformed grid dynamics, displacing synchronous generation and creating new demands for standardized compliance verification. As grid operators increasingly mandate technical performance requirements, including voltage and frequency ride-through, reactive power support, and fault current injection, the need for efficient, scalable, and repeatable testing methodologies has become critical. Traditional on-site and laboratory type tests are costly, time-consuming, and limited in their ability to cover the full spectrum of grid disturbances, driving the adoption of simulation-based approaches as viable pre-certification alternatives.

This thesis develops and validates a Software-in-the-Loop (SIL) compliance testing framework for a Danfoss inverter-based resource model against the EN 50549-2 standard for non-synchronous generating plants connected to medium-voltage distribution networks. The framework integrates the Danfoss Functional Mock-up Unit (FMU) binary into a MATLAB/Simulink co-simulation environment alongside a programmable grid emulator, implementing a black-box input-output verification methodology in which all compliance decisions are derived exclusively from externally observable signals at the point of connection.

Different test categories are executed covering under-voltage and over-voltage ride-through (UVRT/OVRT), frequency ride-through across all EN 50549-2 defined bands, Rate-of-Change-of-Frequency (ROCOF) immunity, active power response to frequency deviation under both Limited Frequency Sensitive Mode overfrequency (LFSM-O) and underfrequency (LFSM-U) modes, reactive power voltage support via Q(U) volt-var characteristic including steady-state accuracy and dynamic step response, and dynamic reactive current injection during asymmetrical faults of three types. Simulation results demonstrate full EN 50549-2 compliance across all tested scenarios: UVRT and OVRT boundary tracking was accurate to within the simulation time-step resolution, LFSM droop errors remained below 0.25 percentage points, Q(U) steady-state accuracy was within $\pm 2\% \, S_{\max}$ across all ten voltage operating points, and asymmetrical fault reactive current errors remained within the EN 50549-2 tolerance band across all five fault scenarios. The framework confirms that a SIL approach can serve as a high-fidelity, repeatable, and computationally efficient alternative to physical pre-certification testing, substantially reducing the time and cost required to identify compliance issues early in the inverter development cycle.

Keywords: Grid codes Compliance, Under Voltage Ride Through, Over Voltage Ride Through, simulation-in-the-loop, Smart Inverter

Contents

List of Figures

List of Tables

Abbreviation	Full Term
AFE	Active Front End
CHIL	Controller Hardware-in-the-Loop
DER	Distributed Energy Resource
DFIG	Doubly-Fed Induction Generator
DLF	Double Line Fault
DLGF	Double Line-to-Ground Fault
DSO	Distribution System Operator
EMS	Energy Management System
ENTSO-E	European Network of Transmission System Operators for Electricity
FMI	Functional Mock-up Interface
FMU	Functional Mock-up Unit
FRT	Fault Ride-Through
GFM	Grid-Forming
HIL	Hardware-in-the-Loop
HVRT	High Voltage Ride-Through
IBR	Inverter-Based Resource
IEC	International Electrotechnical Commission
IEEE	Institute of Electrical and Electronics Engineers
LFSM-O	Limited Frequency Sensitive Mode – Overfrequency
LFSM-U	Limited Frequency Sensitive Mode – Underfrequency
MCB	Main Circuit Breaker
NCRfG	Network Code on Requirements for Grid Connection of Generators
OF	Overfrequency
OFRT	Over-Frequency Ride-Through
OVRT	Over-Voltage Ride-Through
P-HIL	Power Hardware-in-the-Loop
PGU	Power Generating Unit
PHIL	Power Hardware-in-the-Loop
PLL	Phase-Locked Loop
POC	Point of Connection
PV	Photovoltaic
SCR	Short-Circuit Ratio
SIL	Software-in-the-Loop
SLGF	Single Line-to-Ground Fault
SVPWM	Space Vector Pulse Width Modulation
TSO	Transmission System Operator
UF	Underfrequency
UFRT	Under-Frequency Ride-Through
UVRT	Under-Voltage Ride-Through
VRT	Voltage Ride-Through

Acknowledgements

This thesis was carried out at the University of Vaasa in collaboration with Danfoss, and I am deeply grateful to everyone who contributed to its completion.

First and foremost, I would like to express my sincere gratitude to my principal supervisors, Professor Kimmo Kauhaniemi and my personal supervisor Mustafa Alrayah Hassan Ibraheem, for their invaluable guidance, constructive feedback, and continuous encouragement throughout the entire research process.

I would also like to extend my heartfelt thanks to my co-supervisor Shahin Fouladi Panah, whose technical insights, practical advice, and willingness to engage with the details of this work were instrumental in overcoming the many challenges encountered along the way.

I am particularly grateful to Muhammad Khurram Shahzad at Danfoss for providing access to the FMU inverter model and the technical resources necessary to carry out this research. This collaboration gave the thesis a real-world relevance that I value greatly, and I hope the results presented here contribute meaningfully to the ongoing work at Danfoss on grid code compliance verification.

Finally, and most importantly, I wish to thank my family for their unwavering support, patience, and encouragement throughout my studies. Their belief in me has been my greatest source of strength, and this work is as much a reflection of their dedication as it is of my own.

Use of Artificial Intelligence

During the preparation of this thesis, the author used the AI tool Claude Sonnet for grammar checking and writing improvement. The author takes full responsibility for the content of this thesis and confirms that all analysis, interpretations, and conclusions were developed independently by the author.

1 Introduction

Power-system decarbonization is now a central global goal, and it is pushing rapid deployment of carbon-free generation, especially variable renewable energy such as wind and solar. This shift is not just about replacing fuel sources; it is changing the physical and operational character of the grid itself, with planning, management, stability, and control all needing new approaches as systems move toward very high shares of renewables Sajadi, Kenyon, and Hodge (2021). Recent growth data show why this transition matters, in 2025, the deployment of renewable energy technologies continued its strong upward trajectory, with global annual capacity additions reaching approximately $800\,\mathrm{GW}$, representing a 16% increase compared to the previous year as showed in Figure 1. This achievement marked the twenty-third consecutive year of record-breaking growth in renewable energy installations, despite ongoing challenges such as supply chain constraints, delays in grid integration, financial uncertainties, and evolving policy frameworks. Among the newly installed renewable capacity, solar photovoltaic (PV) systems dominated the expansion, contributing more than 75% of total additions. Wind energy represented the second-largest share at approximately 20%, while the remaining capacity was provided by hydropower, bioenergy, geothermal energy, concentrating solar power, and marine energy technologies International Energy Agency (2026).

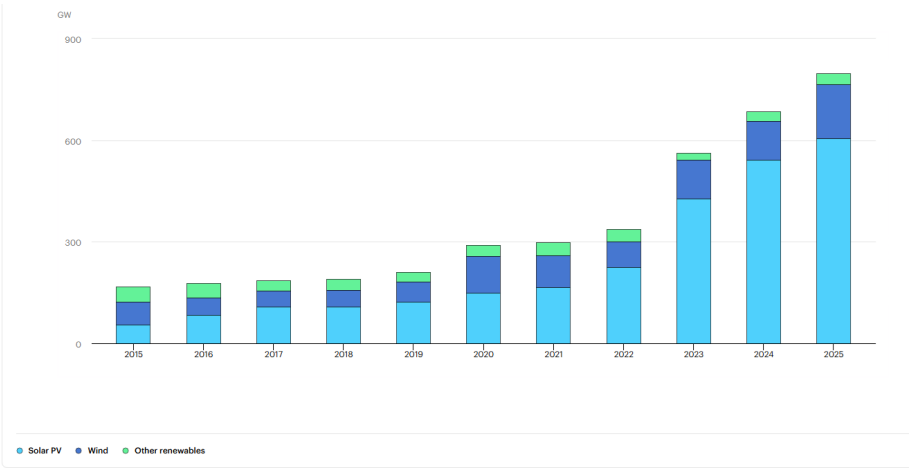

Figure 1. Total renewable capacity additions by technology, 2015-2025 International Energy Agency (2026).

Traditional plants mainly rely on synchronous generators, while solar PV, wind plants, battery storage, and many distributed energy resources are tied to the grid through power electronic inverters, so they are commonly called inverter-based resources. Inverter-based resources (IBRs), such as solar photovoltaics and wind turbines, play a pivotal role in advancing clean electrification by enabling the integration of renewable energy into power grids. These resources, connected through power electronic inverters, offer enhanced controllability and fast response capabilities essential for grid stability amid increasing renewable penetration. Their widespread adoption facilitates decarbonization by replacing fossil fuel-based generation, supporting flexible grid operation, and providing ancillary services like frequency regulation and voltage support. As the power system evolves, IBRs serve as a cornerstone for achieving sustainable, resilient, and low-carbon energy infrastructure Lin et al. (2022).

Here the importance of the grid code compliance comes to ensure the reliable, stable, and secure integration of inverter-based resources into the power grid. As synchronous generators retire, operators can no longer assume that inertia, fault current, voltage support, and disturbance response will appear automatically from the generation mix, so these services increasingly need to be specified as connection and performance requirements for inverter-based resources. That is why many jurisdictions are revising grid codes to require more advanced behavior from wind, solar, batteries, HVDC links, and other converter-based assets, including fault ride-through, reactive power support, frequency response, voltage control, and active power management Yıldırım et al. (2026) Klaes and Fortmann (2025).

A practical example is the move to require grid support functions at both transmission and distribution levels. Under IEEE 1547-2018, inverter-based resources can be required to provide functions such as Volt-Watt, Volt-VAr, Freq-Watt, and voltage/frequency ride-through, so standards are no longer just about safe interconnection but also about supplying ancillary support that helps hold the system together under stress. This shift is important because it links device-level controls directly to system-level reliability outcomes Poudel et al. (2024).

Grid code compliance testing is meant to show that a generating plant, DER unit, or inverter can connect and operate without harming secure system operation, and that it meets the technical behavior required for approval and interconnection. In practice, this verification has a double purpose: plant owners must prove compliance to the network operator, and the network operator must assess that compliance before connection is granted. Because grid-code requirements can be hard to interpret consistently, a clear verification plan is important, and current practice often combines document review, model review, practical tests, simulation studies, and later model validation against measurements from the real plant or device. This is why many compliance frameworks for renewable and inverter-based resources are built around both testing and simulation rather than either one alone Chu, Yuan, Pan, and Hou (2020).

Simulation-based methods for grid code compliance testing offer significant advantages over traditional physical testing, including reduced cost, enhanced safety, and greater scalability. These methods enable comprehensive testing across a wide range of grid conditions and fault scenarios without risking damage to actual equipment or impacting the live grid. Additionally, validated simulation models can accelerate the certification process by allowing early detection of compliance issues and facilitating repeated tests under controlled, repeatable conditions. While simulation may have lower fidelity compared to physical tests, advances in real-time simulation and hardware-in-the-loop techniques help bridge this gap, making simulation an indispensable tool in modern inverter certification frameworks Hafezi, Laaksonen, Kauhaniemi, Lauttamus, and Strandberg (2021).

1.1 Thesis Objectives and Scope

The primary objective of this thesis is to develop and demonstrate a MATLAB/Simulink-based Software-in-the-Loop (SIL) testing framework for evaluating the grid code compliance of a Danfoss inverter-based resource (IBR) model against the requirements specified in the EN 50549-2 standard. Under the European regulatory framework, grid code compliance is a mandatory prerequisite for all Power Generating Modules (PGMs) seeking grid

connection and must be demonstrable through validated simulation models, equipment certificates, or physical testing. Given that traditional on-site type testing is often time-consuming, costly, and limited in its ability to cover the full spectrum of grid disturbances, simulation-based testing has emerged as a cost-effective, repeatable, and scalable alternative that bridges the gap between laboratory certification and field commissioning. This work is bounded by the following technical and procedural constraints:

- Standards compliance: All tests adhere strictly to EN 50549-2 for grid-connected generating modules operating at medium voltage, supplemented by test procedures from EN 50549-10.
- Simulation platform: The entire framework is implemented in MATLAB/Simulink using the SIL methodology; no physical hardware is involved.
- IBR model: The study focuses exclusively on the Danfoss iC7-Hybrid Grid Converter FMU, treated as a compiled black-box component interfaced via the Functional Mock-up Interface (FMI 2.0) standard. Internal controller logic or modifications are outside the scope.
- Grid emulation: A programmable grid emulator generates all required disturbance scenarios. Real-grid interaction and field commissioning are excluded.
- Voltage ride-through testing: Under-voltage (UVRT) and over-voltage (OVRT) tests are executed across EN 50549-2–defined zone-stratified profiles (magnitude vs. duration), assessing grid connection retention and reactive current injection capability.
- Frequency ride-through testing: Under-frequency (UFRT) and over-frequency (OFRT) responses are evaluated under Low-Frequency Sensitivity Mode – Up (LFSM-U) and Down (LFSM-O), per EN 50549-2 active power control requirements.
- ROCOF immunity testing: Rate-of-Change-of-Frequency (ROCOF) tests verify protection relay behavior under rapid frequency transients within EN 50549-2 thresholds.

- Asymmetrical fault response: Dynamic behavior during two-phase (asymmetrical) faults is assessed, with emphasis on positive/negative sequence current injection and post-fault voltage recovery. Three-phase symmetrical faults are excluded.
- Compliance reporting: Results are consolidated into a structured pass/fail compliance matrix aligned with EN 50549-2 limits, intended to serve as a pre-certification documentation basis.

1.2 Literature Review

Cabrera-Tobar, Bullich-Massagué, Aragüés-Peñalba, and Gomis-Bellmunt (2019) develop a local active and reactive power controller for photovoltaic (PV) generators to satisfy modern grid code requirements. Using DIgSILENT PowerFactory simulations, the proposed control strategy is evaluated under varying irradiance and temperature conditions, demonstrating robust power regulation and effective compliance with grid support requirements.

Martínez-Lavín, Villena-Ruiz, Honrubia-Escribano, Hernández, and Gómez-Lázaro (2022) propose an aggregated simulation model for solar photovoltaic power plants aimed at accelerating grid code compliance studies. The model, developed for the Spanish grid code framework, achieves simulation times significantly shorter than detailed plant models while maintaining high accuracy, making it suitable for large-scale compliance assessments.

Nomandela, Mnguni, and Raji (2023) present the modeling and simulation of a large-scale wind power plant using the RSCAD simulation platform. The study evaluates the plant's performance against grid code requirements and demonstrates its capability to contribute to voltage stability and reliable grid integration.

Hashimoto et al. (2021) develop an advanced grid integration testing platform designed to automate compliance testing for distributed renewable energy resources and smart in-

verters. The proposed platform improves testing efficiency, reduces human intervention, and supports the verification of inverter behavior under evolving grid code requirements.

Nanou and Papathanassiou (2014) present a transient simulation model of a grid-connected photovoltaic system designed to satisfy contemporary low-voltage ride-through requirements. The proposed model incorporates converter dynamics and control strategies and is validated through simulations under balanced and unbalanced voltage dip conditions.

Hafezi et al. (2021) investigate the verification of power electronic converter simulation models for grid code compliance testing. The authors compare simulation results with laboratory fault ride-through experiments, demonstrating that averaged converter models can accurately reproduce dynamic responses while reducing testing effort and cost.

Shi et al. (2025) introduce GridCodex, an artificial intelligence framework that employs retrieval-augmented generation (RAG) techniques to support grid code interpretation and compliance assessment. The proposed approach improves the automation and accuracy of regulatory reasoning across multiple grid code documents.

Gashi, Kabashi, Kabashi, Ahmetaj, and Veliu (2012) analyze the compliance of wind farms connected to the Kosovo transmission network using simulation studies. The work focuses on fault ride-through performance, frequency operating limits, and reactive power capability, demonstrating the importance of tailored grid code requirements for wind power plants.

Hafeez (2025) assesses the compliance of a $400\,\mathrm{MW}$ wind power plant with the NEPRA grid code using the PSS/E simulation platform. Through load flow, contingency, and dynamic stability analyses, the study confirms satisfactory voltage recovery, frequency stability, and network performance under grid disturbances.

Jiménez, Gómez-Lázaro, Fuentes, Molina-García, and Vigueras-Rodríguez (2012) validate a doubly-fed induction generator wind turbine model against field measurements and

evaluate wind farm compliance with the Spanish grid code. The results demonstrate accurate representation of electrical variables during fault conditions and successful fulfillment of voltage dip ride-through requirements.

Nomandela, Mnguni, and Raji (2025) investigate the grid-connected operation of a large-scale wind power plant using real-time simulation techniques. The study evaluates compliance with renewable energy grid code requirements and demonstrates improvements in voltage regulation and overall system performance during interconnected operation.

Table 1 summarizes the most relevant studies related to grid code compliance assessment of renewable energy systems. The reviewed literature covers a wide range of technologies, including wind power plants, photovoltaic systems, smart inverters, and power electronic converters. Various approaches have been employed, including detailed electromagnetic simulations, aggregated models, hardware-in-the-loop (HIL) testing, real-time simulation, and laboratory validation.

1.3 Thesis Structure

This thesis is organised into six chapters. Chapter 2 reviews the EN 50549-2 regulatory framework, covering the voltage and frequency operating ranges, ride-through immunity requirements, and active and reactive power control obligations. Chapter 3 describes the SIL co-simulation architecture, introducing the Danfoss iC7-Hybrid Grid Converter FMU and grid emulator integrated into a unified MATLAB/Simulink environment. Chapter 4 presents the test case design and parameter configuration for each of the compliance test categories. Chapter 5 presents the simulation results for all conducted tests with compliance assessments against EN 50549-2 tolerance bands. Chapter 6 concludes the thesis by summarising the key contributions and proposing future research directions, including P-HIL testing and grid-forming inverter compliance verification.

Table 1. Literature Review: Grid Code Compliance Testing Methodologies and Comparison.

Ref.	Study Focus	Simulation Method / Tool	Technology	Key Findings
Cabrera-Tobar et al. (2019)	Active and reactive power control for compliance	DIgSILENT PowerFactory	PV Systems	Demonstrates effective P–Q control under varying conditions
Martínez-Lavín et al. (2022)	Aggregated PV plant model for compliance studies	Aggregated simulation model	PV Power Plants	Achieves high accuracy with reduced simulation time
Nomandela et al. (2023)	Modeling and simulation of large-scale WPPs	RSCAD	Wind Power Plants	Demonstrates grid integration and voltage support capability
Hashimoto et al. (2021)	Automated grid integration testing platform	Integrated testing platform	Smart Inverters	Improves testing efficiency and reduces manual effort
Nanou and Papathanassiou (2014)	Grid-code-compliant PV system modeling	Transient simulation model	PV Systems	Validates LVRT capability under faults
Hafezi et al. (2021)	Verification of converter simulation models	Laboratory validation and simulation	Power Electronic Converters	Demonstrates model-based compliance assessment
Shi et al. (2025)	AI-assisted grid code compliance reasoning	RAG-based AI framework	Generic	Improves automated compliance interpretation
Gashi et al. (2012)	Wind farm compliance assessment	Simulation-based analysis	Wind Turbines	Evaluates FRT and reactive power requirements
Hafeez (2025)	Grid code compliance study of WPPs	PSS/E	Type-4 Wind Turbines	Confirms steady-state and dynamic compliance
Jiménez et al. (2012)	Validation of DFIG models for compliance	Model validation against measurements	Wind Farms	Demonstrates compliance with voltage dip requirements
Nomandela et al. (2025)	Real-time validation of wind plant compliance	Real-time simulation	Large-scale Wind Power Plants	Demonstrates compliance through real-time studies

2 Grid Code Standards and Compliance Requirements

The European grid code framework, established under EU regulations, harmonizes technical requirements for connecting generators, particularly renewables, to transmission and distribution networks, ensuring system stability, security of supply, and integration of inverter-based resources (IBRs) like wind and solar. This includes the Network Code on Requirements for Grid Connection of Generators (NC RfG, Commission Regulation (EU) 2016/631), the EN 50549 series of standards, and implementation guidance from the European Network of Transmission System Operators for Electricity (ENTSO-E). These aim to balance exhaustive EU-level rules (e.g., fault ride-through) with non-exhaustive national

specifications, reducing variability while allowing adaptation to local needs Fortmann et al. (2015).

2.1 EN 50549 Series: Distribution-Level Standards for Non-Synchronous Generation

The EN 50549 series (e.g., EN 50549-1:2019 for requirements up to $800\,\mathrm{kVA}$ and EN 50549-2 for higher capacities) operationalizes the National Codes derived from the EU's Requirements for Generators (RfG) framework for distribution-connected power plants. It specifically targets non-synchronous generation technologies such as photovoltaic inverters and small wind farms. The standard specifies voltage and frequency ride-through profiles, for instance, the ability to remain connected during voltage dips of 5–90% of nominal voltage for durations between $0.2\,\mathrm{s}$ and $180\,\mathrm{s}$. It also mandates reactive current injection proportional to the voltage deviation, with a response magnitude of 90% of rated current initiated within $30\,\mathrm{ms}$. Furthermore, post-fault recovery requirements include resuming at least 90% of pre-fault active power output within $1\,\mathrm{s}$. These provisions are designed to prevent widespread disconnection during grid disturbances and thereby avoid exacerbating system instability Guise et al. (2021) Chmielowiec, Topolski, Piszczek, and Hanzelka (2021) Cerretti, Noce, Rochereau, and Schaupp (2023). Unlike the National Codes derived from the EU's Requirements for Generators (RfG), which focus primarily on transmission-level requirements, the EN 50549 series emphasizes distribution system operator (DSO)-specific tests for power quality (e.g., total harmonic distortion below 5%), anti-islanding protection, and advanced control modes such as reactive power as a function of voltage ($Q(V)$) or power factor as a function of active power ($\cos\varphi(P)$). Non-compliance, such as failure in frequency ranges (47.5–52 Hz) or reactive control activation, can lead to grid disconnection risks, as seen in PV inverter tests Chmielowiec et al. (2021).

2.2 Voltage Ride-Through (VRT) requirements

Voltage ride-through (VRT) requirements, often referred to as Fault Ride-Through (FRT), dictate that power generating units, such as wind turbines and solar photovoltaic (PV) plants, must remain connected to the grid and continue operating during short-term voltage disturbances Kulkarni and Virulkar (2023) Zeb et al. (2022). These requirements are established by grid codes to prevent a ”blackout” or cascading failures that could occur if a large number of renewable energy sources simultaneously disconnected during a fault Kulkarni and Virulkar (2023) Moheb, El-Hay, and El-Fergany (2022).

2.2.1 Under Voltage Ride-Through (UVRT)

UVRT is the capability of a system to withstand significant voltage drops (sags) caused by grid faults like short-circuits or lightning strikes Kulkarni and Virulkar (2023) Zeb et al. (2022). Modern grid codes require the generating unit to stay connected for a specific duration even if the voltage drops to a specific percentage of its rated value. In some countries, including Germany, South Africa, Italy, and Australia, grid codes require generating plants to remain connected to the grid even when the voltage at the point of connection (PoC) drops to 0% of nominal for short durations, typically ranging from $0.15\,\mathrm{s}$ to $0.45\,\mathrm{s}$ Zeb et al. (2022).

Figure 2a, shows the voltage-time curve which is typically divided into three operational zones to structure compliance testing: Area A (normal operation, voltage between 90–110% of nominal voltage, where no dynamic support is needed and generators must operate continuously without disconnection), Area B (the UVRT region where the plant must remain connected and provide support), and Area C (the fault area where the plant may be permitted or required to trip for safety) Bai, Sindhu, and Haque (2023).

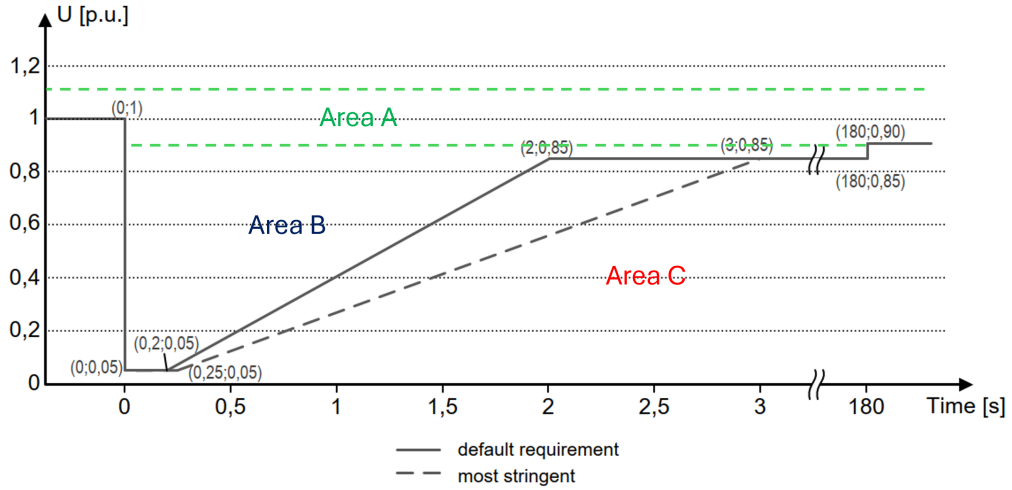

(a) Under-voltage ride-through capability.

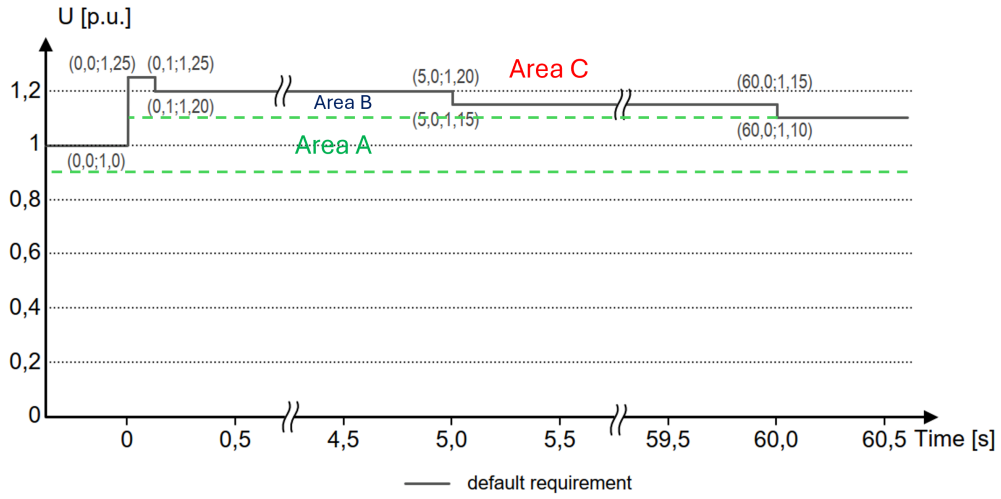

(b) Over-voltage ride-through capability.

Figure 2. Voltage ride-through performance test profiles.

2.2.2 Over-Voltage Ride-Through (OVRT)

also referred to as High-Voltage Ride-Through (HVRT), is the capability of power generating units (PGUs), such as solar photovoltaic (PV) and wind plants, to remain connected to the grid and continue operating during transient voltage increases (swells) Laine (2020). This requirement is essential for maintaining grid stability and preventing cascading failures that could lead to widespread blackouts Kulkarni and Virulkar (2023). Figure 2b shows voltage-time curve that is divided into three distinct operational regions: Area

A, Area B, and Area C. These areas define the mandatory performance of the unit based on the severity and duration of the voltage disturbance. Area A (This area represents the normal operating range of the grid voltage), Area B (the OVRT region where the plant must remain connected and provide support), and Area C (the fault area where the plant may be permitted or required to trip for safety) Bai et al. (2023).

2.3 Operating Frequency Range

In accordance with the EN 50549 regulatory framework, distributed energy resources (DERs) are required to maintain continuous operation within a fundamental frequency range of $49.0\,\mathrm{Hz}$ to $51.0\,\mathrm{Hz}$. This frequency band serves as the standardized baseline for operational stability, ensuring that compliant generating units remains synchronized and active during nominal system fluctuations Chmielowiec et al. (2021) Memon, Karimi, and Kauhaniemi (2022) Hes, Kula, and Svec (2019).

Photovoltaic inverters are required to maintain continuous operation exclusively within the frequency range of $49.0\,\mathrm{Hz}$ to $51.0\,\mathrm{Hz}$. While this constitutes the baseline requirement, the framework permits Transmission System Operators (TSOs) and Distribution System Operators (DSOs) to impose more stringent operational limits based on local grid stability needs Chmielowiec et al. (2021) Hes et al. (2019).

Generating units are required to maintain operational continuity across a frequency spectrum of 47 Hz to 52 Hz until the activation of interface protection systems. To ensure compliance, the plant must sustain operation within defined frequency sub-ranges for the minimum durations and performance criteria SFS-EN-50549-2:2019 (2019).

Table 2 summarizes the EN 50549-2 minimum frequency ride-through requirements. Since real-time execution of the full EN 50549-2 minimum durations, particularly the 30-minute requirements, is computationally impractical within a MATLAB/Simulink SIL simulation environment, the simulation times indicated in Table 2 will follow shorter simulation time

in the experiments made. This approach, in which extended real-world time durations are compressed into shorter simulation windows, is a well-established practice in simulation-based compliance testing and does not compromise the validity of the compliance assessment, provided that steady-state behavior is reached and maintained throughout the simulated event.

Table 2. Frequency operation requirements per EN 50549-2.

Frequency Range	**Time period for operation - Minimum requirement (EN 50549-2)**
47.0 Hz – 47.5 Hz	Not required
47.5 Hz – 48.5 Hz	30 min
48.5 Hz – 49.0 Hz	30 min
49.0 Hz – 51.0 Hz	Unlimited
51.0 Hz – 51.5 Hz	30 min
51.5 Hz – 52.0 Hz	Not required

2.4 Rate of Change of Frequency (ROCOF) Immunity

Rate of Change of Frequency (ROCOF) is defined as the time derivative of the system frequency, commonly expressed as $\frac{df}{dt}$. It is one of the primary indicators of frequency stability Tuo and Li (2020) Muangchuen, Pahasa, and Ngamroo (2023). In a conventional grid, large synchronous generators supply rotational inertia from their spinning masses. That stored kinetic energy gives the system an immediate physical response after a disturbance, slows the early frequency change, and limits ROCOF Kyesswa, Çakmak, Kühnapfel, and Hagenmeyer (2020) Thiesen and Jauch (2021).

This matters more now because wind, solar PV, and many distributed energy resources connect through power electronic converters, which usually do not provide natural synchronous inertia and often decouple any rotating mass from the grid Paturet et al. (2019) Pahasa, Potejana, and Ngamroo (2021). As a result, lower-inertia systems tend to have faster RoCoF and deeper short-term frequency excursions, including lower nadirs, especially in islanded systems and weak grids with many inverter-based DGs Ahmed et al.

(2023) Bustamante, González, Lopez, and Cardona (2023) Farooq and Bass (2022).

ROCOF immunity matters because high ROCOF can cause generating units and DERs to trip, misoperate, or fail to support the grid just when they are most needed. Fast frequency swings can also interfere with protection functions such as under-frequency load shedding and challenge sensitive relays and other equipment Pahasa et al. (2021) Kim and Kim (2024). The impact is not limited to generation tripping. High ROCOF can stress or confuse protection and control schemes, including ROCOF-based loss-of-main protection and under-frequency load shedding, so devices may act too early, too late, or for the wrong reason Misyris, Ramasubramanian, Mitra, and Singhvi (2022) Ally and de Jong (2021).

For DERs in particular, the issue is operational as well as technical. Anti-islanding methods such as vector surge and ROCOF protection are widely used, but if settings are too sensitive they can interrupt the very frequency and voltage support that distributed generation is now expected to provide Matiić, Antić, Havelka, and Capuder (2024). This is why studies have sometimes had to cap nonsynchronous generation share unless ROCOF relays on wind farms and other generators were disabled or adapted Stojković, Lekić, and Stefanov (2020).

2.5 Active Power Response to Frequency deviation

Frequency-active power control is now an explicit grid-code duty, not just a plant option. For wind power plants, TSOs moved from a “produce as much as possible” view to requiring active-power functions such as frequency control and power-gradient limits, with adjustable active power under small frequency deviations. This same logic also appears in PV and DER rules, where active power control must match both resource variation and grid-code frequency response needsR. Khan and Go (2019) Liu, Xu, and Wong (2013). Frequency-active power control requires generating plants to automatically adjust their active power output in proportion to frequency excursions beyond defined thresholds at

the POC. This capability is essential for maintaining the active power balance in the distribution network, since frequency deviations directly reflect imbalances between generation and consumption. EN 50549-2 specifies two distinct active power response modes corresponding to the direction of frequency deviation: the Limited Frequency Sensitive Mode – Overfrequency (LFSM-O) and the Limited Frequency Sensitive Mode – Underfrequency (LFSM-U).

2.5.1 Active Power Response to Overfrequency (LFSM-O)

Under LFSM-O, generating plants are required to reduce their active power output when the grid frequency at the POC exceeds a programmable threshold frequency f_1, which is configurable within the range of $50.2\,\mathrm{Hz}$ to $52\,\mathrm{Hz}$. The power reduction follows a droop characteristic defined by:

$$P_{\max -limit} = P_M - \Delta P = P_M - P_M \cdot \left(\frac{1}{s} \cdot \frac{f - f_1}{f_n} \right) \tag{1}$$

where P_M is the actual active power output at the moment the frequency crosses f_1, f_n is the nominal frequency, f is the actual measured frequency, and s is the programmable droop coefficient, configurable in the range of 2% to 12%. An intentional delay between $0\,\mathrm{s}$ and $2\,\mathrm{s}$ is programmable to prevent unintentional islanding scenarios by avoiding premature power correction during loss-of-mains events.

Figure 3a shows an example of the active power response characteristic of a generating plant to an overfrequency event under LFSM-O, as defined in EN 50549-2, with default parameter settings. As shown, when the grid frequency exceeds the activation threshold, the generating plant begins to reduce its active power output linearly according to the configured droop $s = 5\%$, referenced to the actual power $P_{\mathrm{ref}} = P_M$ at the moment of threshold crossing.

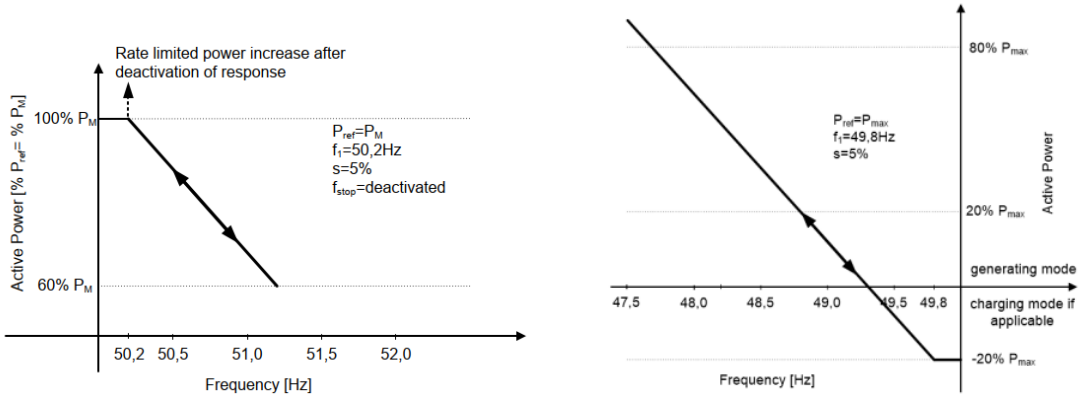

(a) Active power frequency response to overfrequency.

(b) active power frequency response to underfrequency.

Figure 3. Active poewr response to frequency deviation SFS-EN-50549-2:2019 (2019).

2.5.2 Active Power Response to Underfrequency (LFSM-U)

Under LFSM-U, generating plants, particularly electrical energy storage systems (EESS), are required to increase their active power output when the frequency falls below a programmable threshold f_1, configurable in the range of $46.0\,\mathrm{Hz}$ to $49.8\,\mathrm{Hz}$. The active power increase follows a droop function referenced to $P_{\max}$, expressed as:

$$P_{\min\,-limit} = P_M + \Delta P = P_M + P_{max} \cdot \left(\frac{1}{s} \cdot \frac{f_1 - f}{f_n} \right) \tag{2}$$

where the droop s is again configurable from 2% to 12%, and $P_{\max}$ serves as the reference power to enable frequency support even when the generating unit is operating at partial output at the moment the event begins. LFSM-U activation is subject to four simultaneous conditions being met: the unit must be in generating mode, operating below its maximum available active power, within the continuous operating voltage range, and below its current limit.

Figure 3b illustrates the active power response characteristic of a generating plant to an underfrequency event under LFSM-U, with default parameter settings as defined in

EN 50549-2. When the grid frequency drops below the activation threshold $f_1 = 49.8\,\mathrm{Hz}$, the generating plant is required to increase its active power output proportionally, following a droop characteristic of $s = 5\%$ referenced to $P_{\mathrm{ref}} = P_{\mathrm{max}}$. Unlike LFSM-O, where the reference power is the actual output at the moment of threshold crossing, LFSM-U references P_{max} as the baseline to ensure meaningful frequency support even when the generating unit is operating at partial load prior to the underfrequency event.

2.6 Voltage Support by Reactive Power

Since smart inverters can inject or absorb reactive power and often respond faster than voltage regulation equipment, they are useful for managing local voltage variations caused by distributed PV and other inverter-based resources. This is one reason recent standards and grid codes increasingly require or allow DERs to provide voltage regulation support through functions such as Volt-Var Chang and Vanfretti (2024) Darbali-Zamora, Aparicio, Berg, and Gurule (2026).

As per EN 5054-2, generating plants shall not cause voltage changes beyond acceptable limits at the POC, and shall actively contribute to voltage regulation during normal network operation as required by the DSO and the responsible party. The reactive power support capability is required to be maintained throughout the continuous operating frequency range ($49.0\,\mathrm{Hz}$–$51.0\,\mathrm{Hz}$) and voltage range (90%–110% U_C), and the generating plant shall follow the requirements as closely as technically feasible outside these ranges. The default reactive power requirement is up to 33% of P_D, both over-excited and under-excited, when the active power output exceeds 20% of P_D; below this threshold, reactive power shall be provided to a minimum active factor of 0.52.

2.6.1 Q(U) Control Mode

The Q(U) control mode works by using the local POC voltage as the input to a reactive power command, through a piecewise-linear droop curve. The inverter measures volt-

age, looks up the matching point on the curve, and then injects reactive power to raise voltage when it is low or absorbs reactive power to lower voltage when it is high. This lets DERs respond autonomously and continuously to local voltage deviations without waiting for a central command Krishnan, Aftab, Mohammed, Ahmed, and Konstantinou (2025) Almeida, Pasupuleti, Raveendran, and Khan (2021).

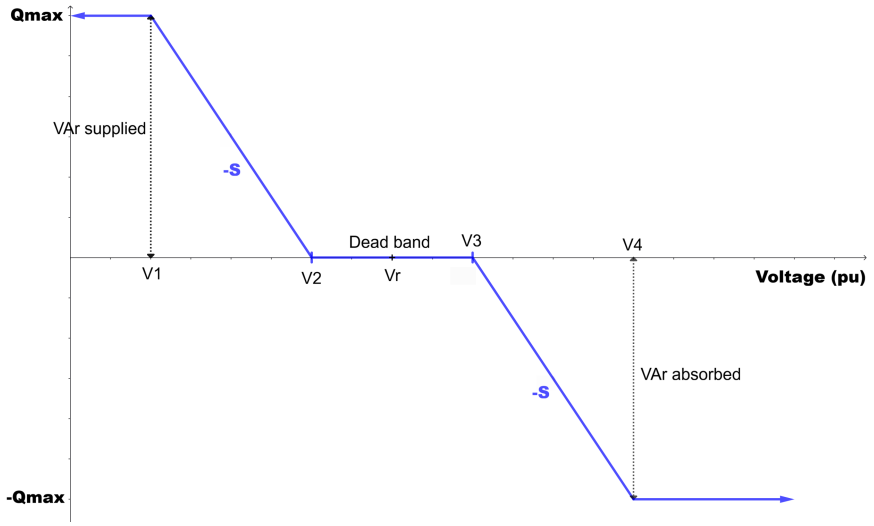

Figure 4. Q(U) control characteristic (Volt-VAr curve).

Figure 4 shows a typical curve that has four voltage points (v_1, v_2, v_3, and v_4) and three operating regions. Below the lower threshold voltage v_2, the inverter injects reactive power (vars), up to a maximum value $Q_{\max}$ at voltage v_1; above the upper threshold voltage v_3, it absorbs reactive power, down to a minimum value $-Q_{\max}$; and between v_2 and v_3 it maintains a deadband where no reactive support is provided because the voltage is already close to the nominal reference v_r. Between these breakpoints, the response is linear with slope s, so the farther the voltage deviates from the acceptable region, the stronger the reactive power response becomes Lee, Yoon, Shin, Kim, and Cho (2020) Almeida, Pasupuleti, and Ekanayake (2021) Zenhom et al. (2025).

To prevent uncontrolled reactive power exchange at low active power output levels, two configurable limiting mechanisms are provided for the $Q(U)$ mode: 1- a minimum $\cos\varphi$ limit, configurable in the range 0–0.95, to cap the reactive current at low active power;

2- Configurable lock-in and lock-out active power thresholds (each in the range 0–100% of design active power P_D), which enable $Q(U)$ mode when active power rises above the lock-in level and disable it when active power falls below the lock-out level, creating a hysteresis band to prevent oscillation.

2.7 Voltage Support During Asymmetrical Faults and Voltage Steps

As converter-based generation has grown, grid operators have started to require distributed generation to provide ancillary support during faults instead of only protecting itself. A notable trend in newer codes is that asymmetrical faults must be handled with explicit sequence-based current injection so voltage support can continue even when the POC voltage is unbalanced. This is why recent and next-generation requirements are framed around positive- and negative-sequence current provision, not just generic reactive current injection Taul, Wang, Davari, and Blaabjerg (2019) Awal et al. (2024).

A common low-voltage ride-through expectation is that the inverter stays connected during the fault and quickly injects reactive current to help recover voltage. Older industrial practice often used balanced positive-sequence control only, but newer rules in countries such as Germany, Austria, and Spain extend this by requiring negative-sequence current injection during asymmetrical faults as well. In practical terms, positive-sequence reactive current is used to support the positive-sequence voltage, while negative-sequence reactive current is used to reduce the negative-sequence voltage and thus help reduce voltage unbalance Marchgraber and Gawlik (2020) Stanojev, Karaca, and Schweizer (2025).

EN 50549-2 clause 4.7.4 defines the short-circuit current requirements for generating plants during faults and sudden voltage steps, going beyond the steady-state reactive power capabilities described in section 4.7 of the EN 50549-2. These requirements mandate that generating plants actively support the network voltage by injecting additional reactive current dynamically within milliseconds of detecting a fault, a function that is independent of the static reactive power control modes.

3 Simulation Environment and IBR Model

A useful way to organize inverter validation is as a testing chain that covers the full range from virtual models to real hardware and finally real-grid operation. In this view, MIL, SIL, CHIL, PHIL, and field tests are not treated as separate islands; they use them in sequence so that each stage checks a different part of the inverter and control stack with increasing realism and cost. This whole-chain view has been described as spanning simulation, SIL, CHIL, PHIL, and field testing sequentially, with the goal of cost-efficient validation across functions and hardwareHeussen et al. (2020) Brandl et al. (2018). The same hierarchy is also framed more broadly as moving across virtual approaches such as simulation, SIL, and co-simulation, real-world approaches such as laboratory and field tests, and mixed approaches such as CHIL and PHIL Strasser et al. (2016). Grid code compliance can be demonstrated using equipment certificates, validated simulation models, and physical tests as seen in figure 5.

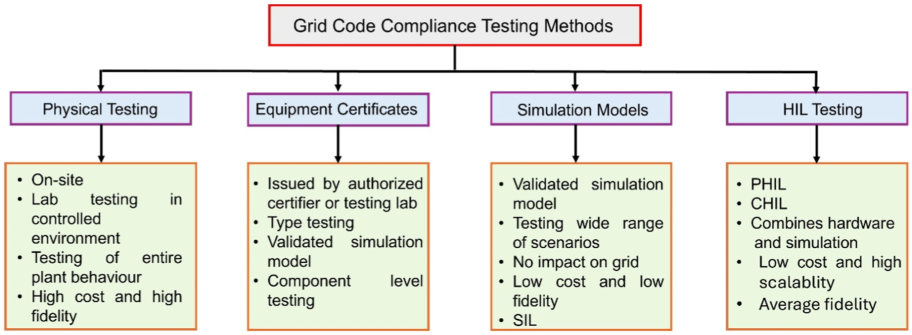

Figure 5. Grid code compliance methods M. K. Khan et al. (2026).

3.1 Simulation-Based Testing

Simulation-based testing is a critical bridge between physical field tests and standardized type tests, offering a low-risk, robust, and cost-effective methodology for verifying grid code compliance. This approach is particularly advantageous when onsite testing is impractical or poses potential risks to grid stability. By employing validated electrical models that replicate plant behavior, incorporating physical characteristics, controller

logic, and electrical interfaces, developers can execute a comprehensive suite of test scenarios without real-world grid impact M. K. Khan et al. (2026). Comparative analyses between simulation outputs and experimental results demonstrated only minor deviations, thereby validating the application of simulation-based testing for formal compliance verification Hafezi et al. (2021).

While simulation-based testing offers significant advantages, including high scalability, broad test coverage, and reduced operational costs, its effectiveness is constrained by factors such as model fidelity, the limited availability of accurate manufacturer-specific models, and the complexities of the validation process. To enhance the accuracy of these virtual assessments, Software-in-the-Loop (SIL) testing has emerged as a more advanced simulation-based methodology for grid code compliance verification.

3.2 Danfoss iC7-Hybrid Grid Converter FMU

The converter model used in this work is fully developed by Danfoss and is provided as a Functional Mock-up Unit (FMU), following the FMI 2.0 (Functional Mock-up Interface 2.0) standard, which defines a tool-independent interface enabling co-simulation between different modelling environments. The FMU encapsulates the actual embedded control firmware of the physical converter, ensuring that the simulation accurately reflects the behaviour of the real hardware without exposing the proprietary control logic, which remains compiled inside a binary library.

The model is initialized via the MATLAB function file, which performs two tasks upon execution: loads all FMU model parameters and initiates the simulation. Parameters can also be configured manually by navigating the model hierarchy: Grid Converter $\rightarrow$ GC1 $\rightarrow$ FMU.

3.2.1 What is FMU

The Functional Mock-up Interface (FMI) standard utilizes a Functional Mock-up Unit (FMU) as a unified digital container enclosing mathematical equations, metadata, and solver configurations that specify the component's interfaces and operational limits. By standardizing this packaging, FMUs allow complex engineering models to be seamlessly imported and executed across any software platform that adheres to the FMI specification. The primary objective of implementing FMU technology is to foster cross-platform interoperability among disparate simulation tools, technical disciplines, and corporate frameworks. In practice, FMUs are deployed under two distinct operational paradigms: Model Exchange, where the hosting simulation tool retains full control over numerical integration and supplies the necessary external differential equation solvers to execute the model; and Co-Simulation, where the FMU operates autonomously with its own embedded numerical solver and exchanges discrete data points with coupled simulation subsystems at predefined communication intervals. Table 3 shows the structure of the components provided within the FMU file MathWorks (2026).

Table 3. FMU Component Structure and Descriptions MathWorks (2026).

Component	Type	Description
`modelDescription.xml`	Mandatory	Defines model identity, all exposed variables (inputs, outputs, parameters), causality, units, and FMI capability flags.
`binaries/<platform>/`	Mandatory	Platform-specific compiled binary (`.dll` on Windows, `.so` on Linux) containing the encapsulated control logic.
`sources/`	Optional	C source and header files, included when the provider opts to share source code.
`resources/`	Optional	Supplementary data files such as lookup tables or parameter maps required at runtime.
`documentation/`	Optional	User manuals, interface diagrams, and integration guides bundled with the FMU.

In the Co-Simulation mode used in this thesis, the FMU operates as an independent computational entity that receives input signals from the MATLAB/Simulink master environment, processes them internally using its encapsulated control logic and solver, and re-

turns output signals. Crucially, the internal implementation of the FMU is not accessible to the user; the binary exposes only the defined input/output interface, making it a true black-box component. This property is particularly relevant in industrial settings where inverter manufacturers such as Danfoss wish to share a validated simulation model of their product with third parties, such as grid operators, certification bodies, or research institutions, without disclosing proprietary control algorithms or firmware source code. The FMI standard thus enables a clear separation between the model provider and the model user, making it the natural interface format for SIL-based grid code compliance testing of commercial inverter products.

3.3 Model Interface: Input Parameters

The Danfoss FMU model parameters are grouped according to the application manual and cover the following main input categories:

1- Basic Parameters, including grid nominal frequency, grid nominal voltage, grid nominal current, DC-link nominal voltage, and unit voltage class;

2- Control Mode and References, encompassing operation mode selection , grid frequency reference source and limits, grid voltage reference, active/reactive current references, DC-link voltage reference, and DC-link current/power references;

3- Limits, comprising grid current limits, grid power limits, and DC-link overvoltage/undervoltage controller levels;

4- Start/Stop Settings, which include start delay, run enable input, pre-charge settings, and main circuit breaker (MCB) control;

5- LCL Filter and Transformer, covering filter voltage feedback source, transformer grid-side and converter-side voltages, transformer phase shift, nominal power, frequency, and

short-circuit impedance.

3.4 Model Interface: Output (Monitoring) Signals

The FMU exposes a comprehensive set of monitoring output signals organized into the following groups:

1- Grid Monitoring, providing grid voltage, grid frequency, grid power factor, grid active power, grid reactive power, and line-to-line voltages;

2- DC-Link Monitoring, reporting DC-link voltage, DC-link current, and DC-link power; Converter Output Monitoring, showing converter output current, output voltage, and output frequency;

3- Control Status, indicated by the Grid Control Status Word which reflects the active operation mode (Island, Droop, PQ, AFE), pre-charge ready status, fault, and warning states;

4- Fieldbus Status Word, reporting converter states including Ready to Switch On, Ready to Run, Running, Fault, Warning, and Run Enabled;

5- Protection and Supervision, which includes heat sink temperature, control unit temperature, grid frequency supervision status word, and up to 10 external temperature protection channels.

In the Simulink model, the key observable output at the top level is the `voltageOut` signal on the DC bus, together with the Grid Connected and Precharge Status LED indicators and the `gridFeedback` signal fed back to the GridInverter block.

3.4.1 Control Logic and Protection

The software manages automatic start and stop sequences, including the internal logic for pre-charging and synchronization before closing the interfacing main circuit breaker. A comprehensive library of supervision functions monitors for grid voltage/frequency deviations, overcurrents, and DC-link overvoltage, triggering configurable responses such as “Stop Modulation” or “Open MCB”.

3.5 Grid Emulator Model

A grid emulator is a programmable, controllable power system representation used in simulation-based compliance testing to reproduce the electrical conditions defined by grid codes, without requiring a direct connection to the physical distribution network. In the context of EN 50549-2 and EN 50549-10 compliance testing, the grid emulator must be capable of generating controlled voltage, frequency, and impedance conditions at the point of connection (POC) to evaluate the response of the generating plant under normal operation, frequency deviations, voltage disturbances, and fault events. The grid emulator model developed in this thesis is implemented in MATLAB/Simulink and consists of three primary components: a programmable three-phase voltage source, a line impedance, and a coupling transformer, together forming a Thevenin-equivalent representation of the MV distribution network seen from the inverter terminals.

3.5.1 Programmable Voltage Source

The backbone of the grid emulator is a three-phase programmable voltage source operating at a nominal line voltage of $12.66\,\mathrm{kV}$, representing the upstream MV distribution network. The source is fully configurable in terms of magnitude, frequency, and phase angle, enabling the emulation of a wide range of grid disturbance scenarios required by EN 50549-2, including steady-state operation at nominal voltage and frequency ($49.0\,\mathrm{Hz}$–$51.0\,\mathrm{Hz}$, 90%–110% U_C), controlled frequency ramps for LFSM-O and LFSM-U

testing across the $47.0\,\mathrm{Hz}$–$52.0\,\mathrm{Hz}$ range, voltage dips and swells for UVRT and OVRT compliance verification, and sudden voltage steps for dynamic reactive current injection testing.

The voltage source is implemented using a controlled three-phase AC source block in Simulink, where the amplitude, frequency, and phase offset can be varied programmatically during the simulation via signal input ports. This allows seamless execution of time-scheduled test sequences without restarting the simulation model.

3.5.2 Line Impedance

A series line impedance is connected between the programmable voltage source and the primary winding of the coupling transformer, representing the equivalent upstream network impedance at the point of connection (PoC). The line impedance captures the resistive and inductive characteristics of the MV feeder and is essential for reproducing the correct voltage drop and short-circuit level seen by the inverter during fault events. The resistance R_{line} and inductance L_{line} are configurable to allow the short-circuit ratio (SCR) at the POC to be stiff grid conditions.

3.5.3 Coupling Transformer

The MV/LV coupling transformer interfaces the $12.66\,\mathrm{kV}$ MV grid emulator with the $690\,\mathrm{V}$ inverter under test. The transformer is modeled as a two-winding transformer with the configuration detailed in Table 4.

The star-grounded primary winding provides a neutral reference on the MV grid side, enabling ground fault current paths and zero-sequence voltage measurement, which is relevant for asymmetrical fault testing. The delta-connected secondary winding isolates the zero-sequence current path on the inverter side, which is a common configuration in MV-connected generating plants and reflects standard industrial practice for inverter-

based resources connected to MV distribution networks.

Table 4. MV/LV Coupling Transformer Parameters.

Parameter	Value
Primary voltage (grid side)	$12.66\,\mathrm{kV}$
Secondary voltage (inverter side)	$690\,\mathrm{V}$
Primary winding connection	Star (Yn)
Secondary winding connection	Delta (D)
Vector group	YnD1

Figure 6 illustrates the topology of the grid emulator model as implemented in MATLAB/Simulink. All key parameters, source voltage magnitude, frequency, impedance values, and transformer ratings, are defined in the model initialization script to allow systematic reconfiguration for each compliance test scenario, ensuring reproducibility and traceability of the simulation results in line with EN 50549-10 verification procedures.

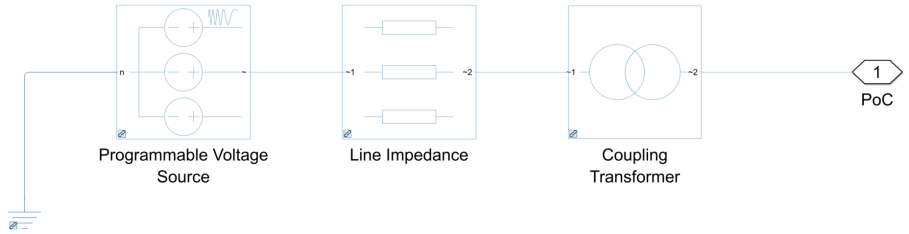

Figure 6. Grid emulator model.

3.6 System Integration and Reference Parameters

The complete simulation model is assembled by integrating three independently developed components into a single closed-loop Simulink environment: the Grid Emulator, the Danfoss FMU inverter model, and the Power Generating Module as seen in Figure 7.

All configurable parameters of the three model components, grid emulator source voltage, line impedance, transformer ratings and FMU initial conditions, are defined in a centralized MATLAB initialization script (`init_model.m`) that runs automatically before the

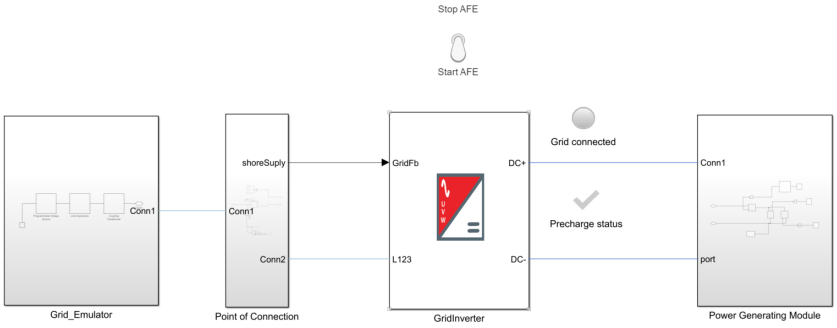

Figure 7. System Integration.

simulation begins via the model's `PreLoadFcn` callback. This ensures that every test scenario starts from a consistent, fully defined initial state and that parameter changes between test cases are applied systematically without risk of stale workspace variables persisting between runs. Table 5 shows the main parameters for the grid, inverter and PGU to enforce consistency between different tested scenarios.

Table 5. Key Simulation Parameters for the Grid Emulator and Inverter Model.

Parameter	**Value**
Grid Emulator Configuration	
Grid voltage (source)	$12.66\,\mathrm{kV}$ (programmable three-phase source)
POC voltage (inverter side)	$690\,\mathrm{V}$ (transformer secondary)
Nominal frequency	$50\,\mathrm{Hz}$
Transformer ratio	$12.66\,\mathrm{kV}$ / $690\,\mathrm{V}$
Transformer connection	Star (grid side) / Delta (inverter side)
Rated phase voltage U_C	$398.37\,\mathrm{V}$ (RMS, phase-to-neutral)
Inverter Model Specifications	
Rated voltage U_c	$690\,\mathrm{V}$
Rated current I_r	$760\,\mathrm{A}$
Rated frequency	$50\,\mathrm{Hz}$
Rated energy capacity	Infinite (ideal DC source approximation)
Internal resistance	$10\,\mathrm{m\Omega}$

4 Test Design and Grid Code Parameters Configuration

4.1 Overview and Black-Box Testing Philosophy

The Danfoss inverter model, delivered as a compiled FMU, is treated as a black-box system throughout the compliance testing process. Its internal control architecture, protection logic, and software parameters are modified before the simulation. The methodology therefore adopts an input-output compliance verification approach: controlled and well-defined grid disturbance stimuli are applied at the POC through the grid emulator, and the inverter's externally observable output signals are measured, processed, and evaluated against the quantitative requirements of EN 50549-2. Compliance is established entirely from the external signal behaviour, without any assumption about internal implementation.

4.2 Methodology

Figure 8 illustrates the overall compliance test process applied in this thesis to evaluate the Danfoss FMU inverter model against the requirements of EN 50549-2. The process is structured as a single coordinated simulation campaign in which four independent test groups are executed in parallel from a common steady-state starting point, with all results consolidated into a final compliance report.

The process begins with a configuration step in which the steady-state operating parameters and grid code thresholds are defined and loaded into the simulation model. This includes the grid emulator settings (source voltage, line and transformer configurations), the FMU initial conditions, and all EN 50549-2 compliance boundaries. The voltage V, frequency f, and current I are continuously monitored at the POC. These recorded signals form the input dataset for all test groups, and based on these signals, all other required quantities are calculated, such as active power, reactive power, sequence current,

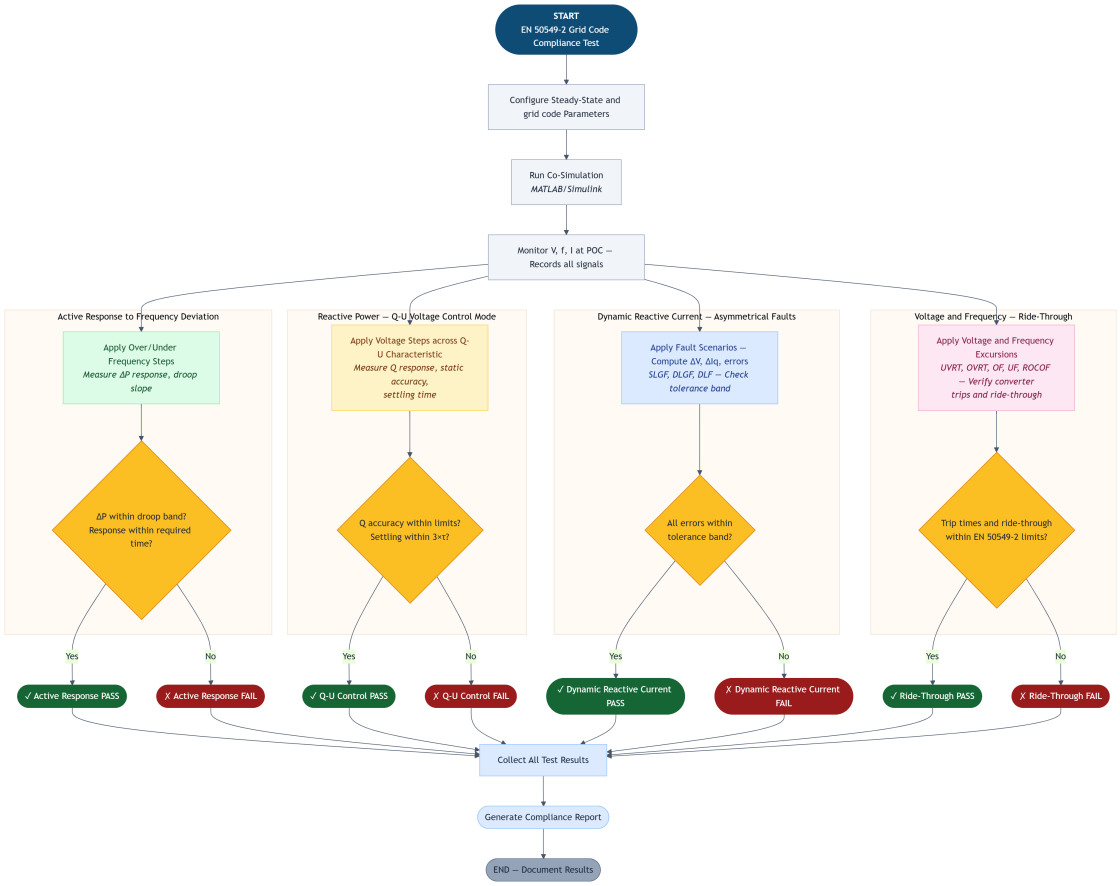

Figure 8. Compliance process flowchart.

sequence voltage, etc.

From the common monitoring node, the process branches into four independent test groups, each targeting a distinct set of EN 50549-2 requirements.

Voltage and Frequency Ride-Through: Voltage and frequency excursions covering UV, OV, OF, UF, and ROCOF scenarios are applied. The FMU's connection times and ride-through behaviour are evaluated against the EN 50549-2 compliance boundary curves. The compliance decision checks whether the FMU remains connected throughout must-stay-connected scenarios or not.

Reactive Power Q(U) Voltage Control Mode: Controlled voltage steps are applied across the configured Q(U) characteristic. The reactive power response of the FMU is measured,

and the static accuracy, settling time, and dynamic trajectory are evaluated. The compliance decision checks whether the reactive power accuracy remains within $\pm 2\%$ of $S_{\max}$ and whether the settling time is consistent with the configured first-order filter time constant τ, i.e., full settling within approximately 3τ as required by EN 50549-2.

Active Response to Frequency Deviation: Over-frequency and under-frequency steps are applied via the grid emulator. The active power response ΔP, droop slope, dead time and response time are calculated. The compliance decision checks whether the active power deviation falls within the required droop band and whether the response is achieved within the required time limits defined in EN 50549-2.

Dynamic Reactive Current under Asymmetrical Faults: Three asymmetrical fault scenarios are applied, single-line-to-ground fault (SLGF), double-line-to-ground fault (DLGF), and double-line fault (DLF). For each scenario, the positive and negative sequence voltage deviations ΔU_1 and ΔU_2 are computed, the required reactive current injections I_{Q1} and I_{Q2} are derived and compared with the EN 50549-2 k-factor equations, and the actual FMU current response is compared against the tolerance band of EN 50549-2. The compliance decision checks whether all sequence current errors remain within the defined $\pm$tolerance band.

Each of the test groups produces an independent pass or fail outcome based on its compliance decision. A compliance report is then generated documenting the outcome of each test group, the supporting signal plots, and the quantitative compliance metrics. The process concludes with the documentation of the final results, providing a structured evidence base for EN 50549-2 compliance assessment of the Danfoss FMU inverter model.

Table 6. Key Breakpoints of the UVRT Compliance Boundary.

Breakpoint (t; V)	Time [s]	Technical Interpretation
(0; 1.0)	$t = 0$	At the instant of fault inception, the pre-fault voltage is 1.0 p.u.
(0; 0.05)	$t = 0$	The boundary drops instantaneously to 0.05 p.u., meaning the inverter must tolerate any voltage above 0.05 p.u. from the very onset of the fault.
(0.2; 0.05)	$t = 0.2$	The inverter must remain connected as long as the voltage stays above 0.05 p.u. for any duration up to 0.2 s.
(2; 0.85)	$t = 2$	The boundary ramps linearly from 0.05 p.u. at $t = 0.2$ s to 0.85 p.u. at $t = 2$ s. For slowly recovering dips, the minimum required connected duration increases progressively with dip depth.
(3; 0.85) / (3; 0.9)	$t = 3$	Between $t = 2$ s and $t = 3$ s, the boundary steps from 0.85 p.u. to 0.9 p.u. Thereafter, the inverter must remain connected indefinitely at voltages above 0.9 p.u.

4.3 UVRT and OVRT Threshold Profiles

The UVRT compliance boundary for non-synchronous generating technology is defined in EN 50549-2 clause 4.5.3.2 as a voltage-time profile that specifies the minimum duration for which the inverter must remain connected at any given per-unit voltage level below the continuous operating range. The UVRT boundary profile used in this model that is fully inspired by the EN 50549-2 is defined by five key breakpoints as seen in Figure 9a and described in table 6.

The OVRT compliance boundary is defined in EN 50549-2 clause 4.5.4 as a voltage-time profile specifying the minimum duration the inverter must remain connected at any given per-unit overvoltage level above the continuous operating range.

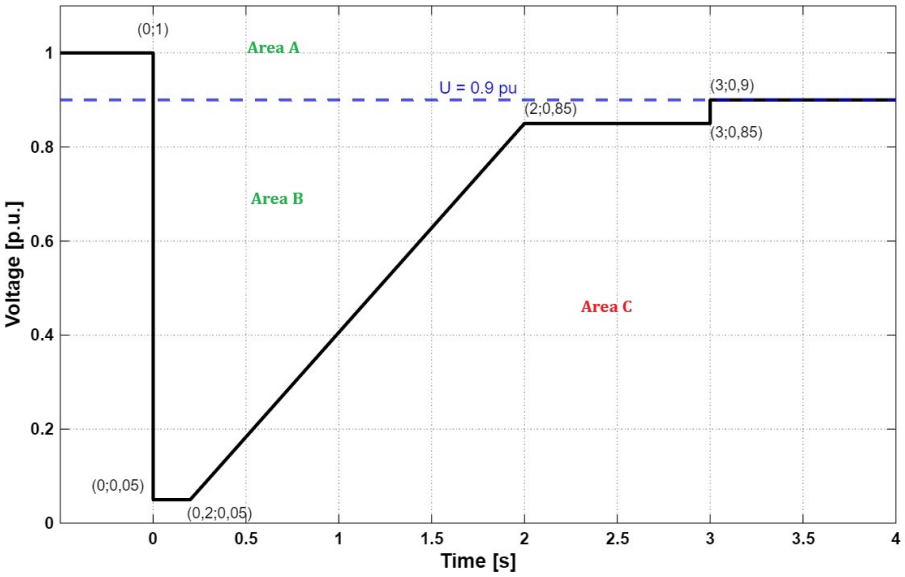

(a) Under-voltage ride-through profile.

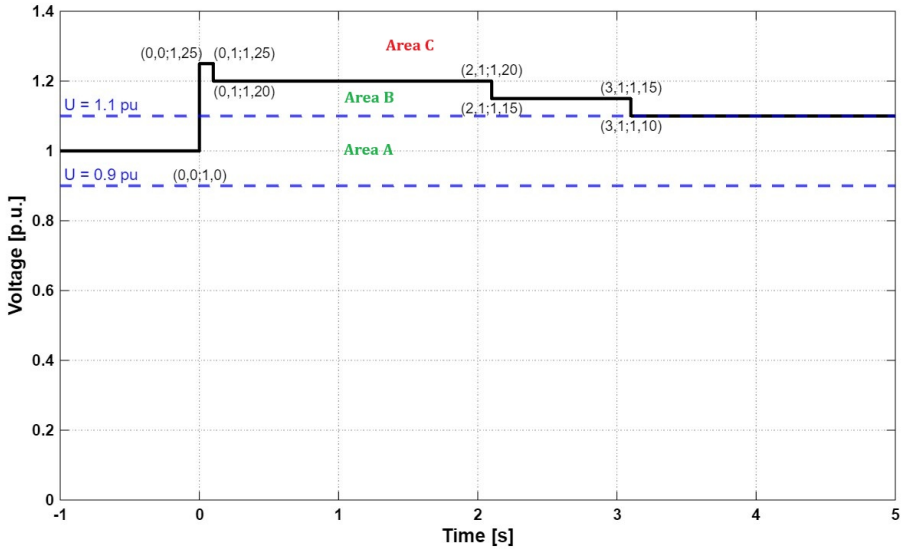

(b) Over-voltage ride-through profile.

Figure 9. Voltage ride-through profiles.

Table 7. Key Breakpoints of the EN 50549-2 OVRT Compliance Boundary.

Breakpoint (t; V)	Time [s]	Technical Interpretation
(0; 1.0)	$t = 0$	Pre-swell condition at nominal voltage 1.0 p.u.
(0; 1.25) / (0.1; 1.25)	$t = 0 \rightarrow 0.1$	The inverter must remain connected at voltages up to 1.25 p.u. for durations up to 0.1 s. This represents the most extreme permissible overvoltage.
(0.1; 1.20) / (2.1; 1.20)	$t = 0.1 \rightarrow 2.1$	For voltages up to 1.20 p.u., the inverter must stay connected for durations up to approximately 2 s.
(2.1; 1.15) / (3.1; 1.15)	$t = 2.1 \rightarrow 3.1$	For voltages up to 1.15 p.u., the inverter must remain connected for durations up to approximately 3 s.
(3.1; 1.10)	$t \geq 3.1$	For voltages at or below 1.10 p.u., the inverter must remain connected indefinitely, as this corresponds to the upper boundary of the continuous operating range.

The OVRT boundary profile used in this model that is fully inspired by the EN 50549-2 is defined by breakpoints as seen in Figure 9b and described in table 7.

The two dashed blue reference lines at $U = 0.9$ p.u. and $U = 1.1$ p.u. shown in Figure 9 bound the continuous normal operating voltage band from EN 50549-2 clause 4.4.4. Any operating point above or low these upper and lower normal operating limits and within the stay-connected region, the inverter must not trigger a trip until the time exceed the minimum must stay connected time.

4.4 OF and UF threshold limits

EN 50549-2 clause 4.4.2 divides the frequency operating range into six zones, symmetric around the nominal $50\,\mathrm{Hz}$. Table 8 presents the EN 50549-2 minimum requirement for each zone together with the simulation time used to exercise it.

Table 8. Frequency Operating Zones and Simulation Requirements.

Frequency Range	EN 50549-2 Minimum Requirement	Simulation minimum Time
$47.0\,\mathrm{Hz}$ – $47.5\,\mathrm{Hz}$	Not required	$1\,\mathrm{s}$
$47.5\,\mathrm{Hz}$ – $48.5\,\mathrm{Hz}$	$30\,\mathrm{min}$	$2\,\mathrm{s}$
$48.5\,\mathrm{Hz}$ – $49.0\,\mathrm{Hz}$	$30\,\mathrm{min}$	$3\,\mathrm{s}$
$49.0\,\mathrm{Hz}$ – $51.0\,\mathrm{Hz}$	Unlimited	Unlimited
$51.0\,\mathrm{Hz}$ – $51.5\,\mathrm{Hz}$	$30\,\mathrm{min}$	$3\,\mathrm{s}$
$51.5\,\mathrm{Hz}$ – $52.0\,\mathrm{Hz}$	Not required	$1\,\mathrm{s}$

The normal operating zone of $49.0\,\mathrm{Hz}$–$51.0\,\mathrm{Hz}$ requires unlimited continuous connection, the inverter must never trip within this band under any circumstances. The adjacent zones at $47.5\,\mathrm{Hz}$–$48.5\,\mathrm{Hz}$ (under-frequency) and $51.0\,\mathrm{Hz}$–$51.5\,\mathrm{Hz}$ (over-frequency) both carry a minimum stay-connected requirement of $30\,\mathrm{min}$, reflecting that these conditions may occur for extended periods during grid disturbances without justifying disconnection. The outermost zones at $47.0\,\mathrm{Hz}$–$47.5\,\mathrm{Hz}$ and $51.5\,\mathrm{Hz}$–$52.0\,\mathrm{Hz}$ carry no mandatory minimum connection time, meaning the inverter is permitted to trip immediately once the frequency enters these extreme bands, although it is not required to do so.

Since directly simulating $30\,\mathrm{min}$ frequency excursions in a co-simulation environment is computationally impractical, the simulation times in Table 8 are chosen as representative durations that are sufficient to confirm stable ride-through behaviour within each zone. A simulation minimum time of $2\,\mathrm{s}$ is required for the $47.5\,\mathrm{Hz}$–$48.5\,\mathrm{Hz}$ zone and $3\,\mathrm{s}$ for the $48.5\,\mathrm{Hz}$–$49.0\,\mathrm{Hz}$ and $51.0\,\mathrm{Hz}$–$51.5\,\mathrm{Hz}$ zones, providing enough resolution to observe the FMU's steady-state connected behaviour and confirm the absence of spurious tripping. For the outermost zones where connection is not required, a simulation required time of $1\,\mathrm{s}$ is needed to verify that the FMU handles the transition into the extreme frequency band without an uncontrolled fault response.

4.5 Voltage Support by Reactive Power Parameter Configuration

The Q(U) voltage-related control mode is defined in EN 50549-2 clause 4.7.2.3.3 as the primary mechanism by which the generating plant regulates its reactive power output

as a continuous piecewise-linear function of the measured terminal voltage. Before conducting the Q(U) compliance tests, all configurable parameters of the Q(U) characteristic must be set within the ranges permitted by EN 50549-2 and then fixed for the duration of the test campaign. Table 9 summarises the standard-permitted range for each parameter alongside the configured value adopted in this thesis.

Table 9. Q(U) Control Parameters: Standard Ranges and Configured Values.

Parameter	Standard Range (EN 50549-2)	Configured Value
HV Start	Configurable	$103\%\,U_n$
HV Maximum Reactive	0 – $33\%\,P_D$	$33\%\,P_D$
HV Reactive Slope	Configurable	$5\%/\%$
LV Start	Configurable	$97\%\,U_n$
LV Maximum Reactive	0 – $33\%\,P_D$	$33\%\,P_D$
LV Reactive Slope	Configurable	$5\%/\%$
Reactive Power Displacement	Configurable	0
Time Constant T_c	$3\,\mathrm{s}$ – $60\,\mathrm{s}$	$3\,\mathrm{s}$
Minimal $\cos\phi$	0.0 – 0.95	0.9
Lock-in Power Level	0 – $100\%\,P_D$	$20\%\,P_D$
Lock-out Power Level	0 – $100\%\,P_D$	$15\%\,P_D$

4.5.1 Characteristic Curve Configuration

The Q(U) characteristic is configured as a symmetric deadband curve centred on nominal voltage, with activation thresholds at $97\%\,U_n$ on the low-voltage side (LV Start) and $103\%\,U_n$ on the high-voltage side (HV Start) as shown in Figure 10 and summarized in equation 3. Within this $\pm 3\%$ deadband, the reactive power output is held at the displacement setpoint, which is set to zero in this configuration, meaning no reactive power offset is injected during nominal voltage conditions. Outside the deadband, the reactive power ramps linearly with a slope of 5% reactive power per 1% voltage deviation on both the LV and HV sides, up to a maximum reactive power exchange of $33\%\,P_D$ in both the over-excited and under-excited directions. This maximum value corresponds to the upper boundary of the EN 50549-2 clause 4.7.2.2 reactive power capability range, which permits up to $0.33\,Q/P_D$ in both directions.

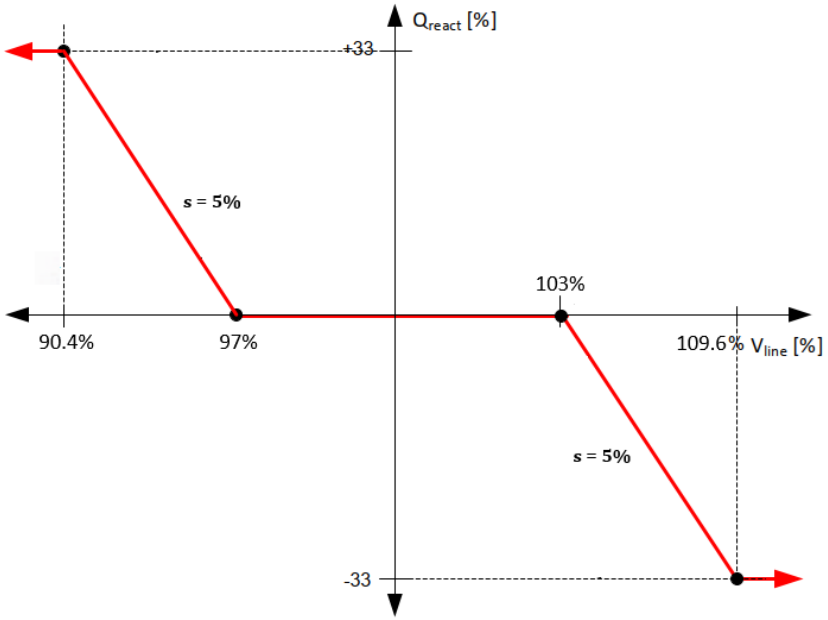

Figure 10. Volt-VAr configured curve.

$$\Delta Q = \begin{cases} +33\%, & V \leq 90.4\% \\ 5(97 - V)\%, & 90.4\% < V < 97\% \\ 0\%, & 97\% \leq V \leq 103\% \\ -5(V - 103)\%, & 103\% < V < 109.6\% \\ -33\%, & V \geq 109.6\% \end{cases} \tag{3}$$

4.5.2 Dynamic Response Configuration

The dynamics of the Q(U) control are governed by a first-order low-pass filter with a configurable time constant in the range of $3\,\mathrm{s}$ to $60\,\mathrm{s}$ as specified in EN 50549-2 clause 4.7.2.3.3. In this thesis, the time constant is set to its minimum permissible value of $T_c = 3\,\mathrm{s}$, which produces the fastest compliant response. Under this setting, the FMU is expected to complete approximately 95% of any reactive power step change within $3 \times T_c = 9\,\mathrm{s}$ following a voltage step. The dynamic compliance tolerance band permits a deviation of up to $\pm 5\%\, P_D$ from the ideal first-order filter trajectory, together with a

time delay tolerance of up to $3\,\mathrm{s}$ relative to the ideal response, as defined in EN 50549-2 clause 4.7.2.3.3.

4.5.3 Lock-in and Lock-out Power Levels

To prevent unnecessary reactive power exchange at very low active power outputs, EN 50549-2 clause 4.7.2.3.3 requires the Q(U) mode to include a hysteresis activation mechanism defined by two configurable active power thresholds. The lock-in level is set to $20\%\ P_D$, meaning the Q(U) control activates only once the FMU's active power output rises above this threshold. The lock-out level is set to $15\%\ P_D$, meaning the Q(U) control deactivates and holds its last reactive power value if the active power subsequently falls below this lower threshold. The lock-in level being higher than the lock-out level creates a hysteresis band of $5\%\ P_D$ that prevents rapid toggling of the Q(U) mode around the activation boundary.

4.5.4 Minimum Power Factor Limit

The minimal $\cos\phi$ is configured at 0.9, which is within the limits defined in EN 50549-2 clause 4.7.2.3.3. This setting constrains the minimum power factor that the FMU may operate at as a consequence of the Q(U) reactive power injection. In practice, it acts as a reactive power ceiling: if the Q(U) characteristic would prescribe a reactive power level that pushes the operating power factor below 0.9, the reactive output is limited to the value corresponding to $\cos\phi = 0.9$ at the current active power level.

4.6 LFSM-O and LFSM-U Parameter Configuration

The active power response to frequency deviation is defined in EN 50549-2 clauses 4.6.1 and 4.6.2 for over-frequency (LFSM-O) and under-frequency (LFSM-U), respectively. Both modes operate on a droop principle: once the measured frequency at the POC crosses the

configured activation threshold f_1, the FMU is required to modify its active power output proportionally to the frequency deviation, following the programmed droop characteristic. Table 10 summarises the EN 50549-2 parameter ranges alongside the configured values used in this thesis for both LFSM-O and LFSM-U.

Table 10. LFSM-O and LFSM-U Control Parameters: Standard Ranges and Configured Values.

Parameter	EN 50549-2 Range	LFSM-O Configured	LFSM-U Configured
Activation Threshold f_1	OF: $50.2\,\mathrm{Hz}$–$52.0\,\mathrm{Hz}$ / UF: $49.8\,\mathrm{Hz}$–$46.0\,\mathrm{Hz}$	$50.2\,\mathrm{Hz}$	$49.8\,\mathrm{Hz}$
Droop s	2% – 12%	5%	5%
Reference Power P_{ref}	OF: P_M / UF: $P_{\max}$	$P_M = 0.5$ p.u.	$P_{\max} = 1.0$ p.u.
Intentional Delay	$0\,\mathrm{s}$ – $2\,\mathrm{s}$ (default: $0\,\mathrm{s}$)	$0\,\mathrm{s}$	$0\,\mathrm{s}$
Deactivation Threshold f_{stop}	$50.0\,\mathrm{Hz}$ – f_1 (default: deactivated)	Deactivated	Deactivated

The activation threshold f_1 is set to the EN 50549-2 default value of $50.2\,\mathrm{Hz}$ for LFSM-O and $49.8\,\mathrm{Hz}$ for LFSM-U, corresponding to the minimum configurable threshold in each direction. These values place the activation boundary at the edge of the nominal continuous operating range ($49.0\,\mathrm{Hz}$–$51.0\,\mathrm{Hz}$), ensuring the frequency response activates as soon as the frequency leaves this band. Both LFSM-O and LFSM-U are configured with a droop of $s = 5\%$, which is the EN 50549-2 default value. The droop defines the proportional relationship between the per-unit frequency deviation and the required per-unit active power change, relative to the reference power P_{ref}.

The reference power P_{ref} differs between the two modes by design of the standard. For LFSM-O, EN 50549-2 clause 4.6.1 specifies that for non-synchronous generating technology $P_{\text{ref}} = P_M$, the actual active power at the instant the frequency crosses f_1. In this thesis, the active power during the over-frequency test is held at a steady-state value of $P_M = 0.5$ p.u., so the LFSM-O droop calculation uses this pre-event power level as its reference. For LFSM-U, EN 50549-2 clause 4.6.2 specifies that $P_{\text{ref}} = P_{\max}$ regardless of the instantaneous operating point, so that the inverter can provide upward frequency support even when initially operating at partial load. Accordingly, $P_{\max} = 1.0$ p.u. is used as the LFSM-U reference, representing the full rated active power capability of the FMU.

The intentional delay is set to $0\,\mathrm{s}$ for both modes, meaning the FMU is expected to begin responding to frequency deviation as fast as technically feasible from the instant f_1 is

crossed, with a maximum permitted dead time of $2\,\mathrm{s}$ and a step response time of $30\,\mathrm{s}$ as specified in EN 50549-2 clauses 4.6.1 and 4.6.2. The deactivation threshold f_{stop} is left deactivated for both modes.

4.7 Dynamic Response for Asymmetrical Fault

The dynamic reactive current requirement for non-synchronous generating technology is defined in EN 50549-2 clause 4.7.4.2.1. During fault conditions or sudden voltage jumps, the FMU is required to inject additional reactive current in the positive and negative sequence, proportional to the measured sequence voltage deviations from the pre-fault baseline. Before the asymmetrical fault tests are conducted, all configurable parameters governing the activation, sensitivity, and gradient of this response must be fixed. Table 11 summarises the EN 50549-2 permitted ranges alongside the configured values adopted in this thesis.

Table 11. Dynamic Reactive Current Parameters: Standard Ranges and Configured Values.

Feature	EN 50549-2 Standard Range	Configured Value
Static Voltage Range (Undervoltage)	80% – $100\%\,U_c$	$95\%\,U_c$
Static Voltage Range (Overvoltage)	100% – $120\%\,U_c$	$105\%\,U_c$
k_1 and k_2 Gradients	2 – 6	$k = 2$
Insensitivity Range	0% – $15\%\,U_c$ (default: 5%)	0%
Deactivation Time (no static breach)	$5\,\mathrm{s}$	$5\,\mathrm{s}$
Sudden Jump Baseline	50 periods ($1\,\mathrm{s}$)	$1\,\mathrm{s}$

The static voltage range defines the outer boundary of the normal operating zone used by the dynamic reactive current function to determine whether a fault condition is active. If any phase-to-phase voltage falls outside this range, the dynamic reactive current provision is activated regardless of whether the voltage change meets the sudden-jump criterion. The undervoltage boundary is configured at $95\%\,U_c$, which is tighter than the minimum configurable value of $80\%\,U_c$. The overvoltage boundary is configured at $105\%\,U_c$. The default static voltage range, if no setting is provided by the DSO, is the continuous operating voltage range of 90%–$110\%\,U_c$ as defined in EN 50549-2 clause 4.4.4.

The insensitivity range defines a voltage deviation threshold below which the dynamic reactive current function neither requires nor prohibits additional reactive current injection. It is configured at 0%, removing the insensitivity dead zone entirely, so that any measurable positive- or negative-sequence voltage deviation immediately engages the reactive current requirement.

If the dynamic reactive current function is triggered by a sudden voltage jump that does not cause any phase-to-phase voltage to exceed the static voltage range boundaries, EN 50549-2 clause 4.7.4.2.1 requires the function to deactivate after $5\,\mathrm{s}$.

The sudden voltage jump is defined in EN 50549-2 clause 4.7.4.2.1 as the absolute difference between the current positive- or negative-sequence voltage and the 50-period ($1\,\mathrm{s}$) running average of that sequence voltage.

5 Simulation Results and Compliance Analysis

5.1 UVRT Results

Four test scenarios were executed to evaluate the FMU's under-voltage ride-through behaviour across the full voltage-time compliance boundary defined in EN 50549-2 clause 4.5.3.2 for non-synchronous generating technology. The scenarios collectively cover the continuous operating zone (Area A), the mid-depth transient region (Area B), and the sub-threshold (Area C) condition of the UVRT characteristic as seen in Figure 11. In each case, three signals were recorded simultaneously: the measured terminal voltage in per unit, the EN 50549-2 UVRT boundary curve evaluated at the current time instant, and the FMU trip signal. Compliance requires the trip signal to remain de-asserted (logic 0) for the entire duration that the voltage-time operating point lies above the boundary curve, and to assert (logic 1) once the operating point crosses into Area C below the boundary.

The first scenario shown in Figure 11a applied a voltage reduction (0.95 p.u.) that remained above 0.9 p.u., placing the operating point within the EN 50549-2 continuous operating voltage range. No ride-through event was triggered and the trip signal remained at logic 0 throughout, confirming that the FMU does not issue spurious trips under normal operating voltage reductions.

In the second scenario shown in Figure 11b, the voltage was reduced to 0.85 p.u. and held beyond the minimum required duration. The FMU remained connected with the trip signal at logic 0 for exactly $2\,\mathrm{s}$, satisfying the EN 50549-2 minimum stay-connected requirement at this voltage level. Once the $2\,\mathrm{s}$ limit was exceeded and the operating point crossed into Area C below the UVRT boundary, the FMU correctly asserted the trip signal, confirming that the disconnection was both timely and compliant.

The third scenario reduced the voltage to approximately 0.6 p.u. as seen in Figure 11c, for which linear interpolation of the EN 50549-2 boundary ramp between the breakpoints

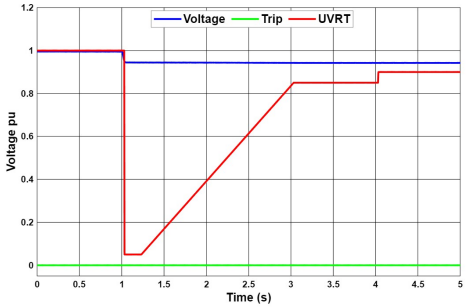

(a) Scenario 1: Voltage reduction to 0.95 p.u.

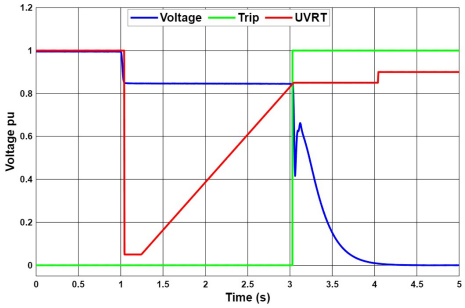

(b) Scenario 2: Voltage dip to 0.85 p.u.

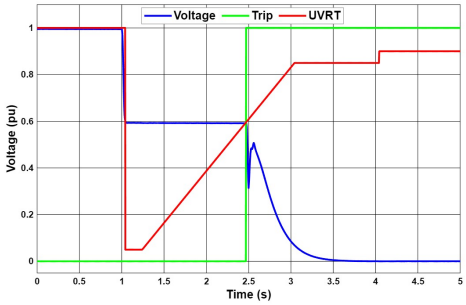

(c) Scenario 3: Voltage dip to ≈ 0.6 p.u.

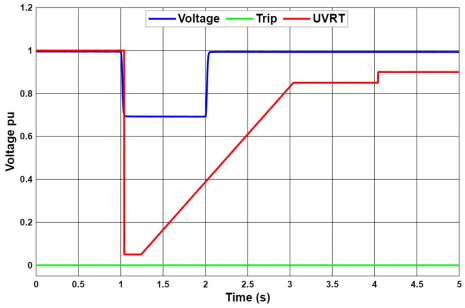

(d) Scenario 4: Voltage dip to 0.7 p.u. for 1 s.

Figure 11. UVRT Compliance Verification.

(0.2 s; 0.05 p.u.) and (2 s; 0.85 p.u.) yields a minimum required connection duration of approximately $1.38\,\mathrm{s}$. The FMU remained connected for a measured $1.437\,\mathrm{s}$ before the operating point entered Area C and the trip signal was correctly asserted.

The fourth scenario applied a dip to 0.7 p.u. for $1\,\mathrm{s}$ as can be seen in Figure 11d, which is shorter than the minimum required duration of approximately $1.56\,\mathrm{s}$ at that voltage level. Since the operating point remained above the UVRT boundary for the entire event, no trip was permissible or observed; voltage was then restored to 1.0 p.u. and the FMU resumed normal operation without asserting a trip, consistent with the EN 50549-2 requirement to recover at least 90% of pre-fault active power within $1\,\mathrm{s}$ following return to the continuous operating range.

The results across all four scenarios are summarised in Table 12. All four scenarios produced a passing result. Test cases 2 and 3 demonstrate that the FMU correctly remains

connected for at least the EN 50549-2 minimum required duration before tripping upon entry into Area C, while test cases 1 and 4 confirm that no spurious tripping occurs when the voltage-time operating point remains above the boundary curve.

Table 12. UVRT Compliance Test Results Summary.

Test Case	Voltage Level	Duration Applied	Min. Required time	Trip Behaviour	Result
1	> 0.9 p.u.	$4\,\mathrm{s}$	Continuous operation	No trip (above boundary)	PASS
2	0.85 p.u.	$> 2\,\mathrm{s}$	$2\,\mathrm{s}$	Trip at $2\,\mathrm{s}$ (entered Area C)	PASS
3	≈ 0.6 p.u.	$> 1.437\,\mathrm{s}$	$\approx 1.437\,\mathrm{s}$	Trip at $1.437\,\mathrm{s}$ (entered Area C)	PASS
4	0.7 p.u.	$1\,\mathrm{s}$ ($<$ required)	$\approx 1.56\,\mathrm{s}$	No trip (above boundary throughout)	PASS

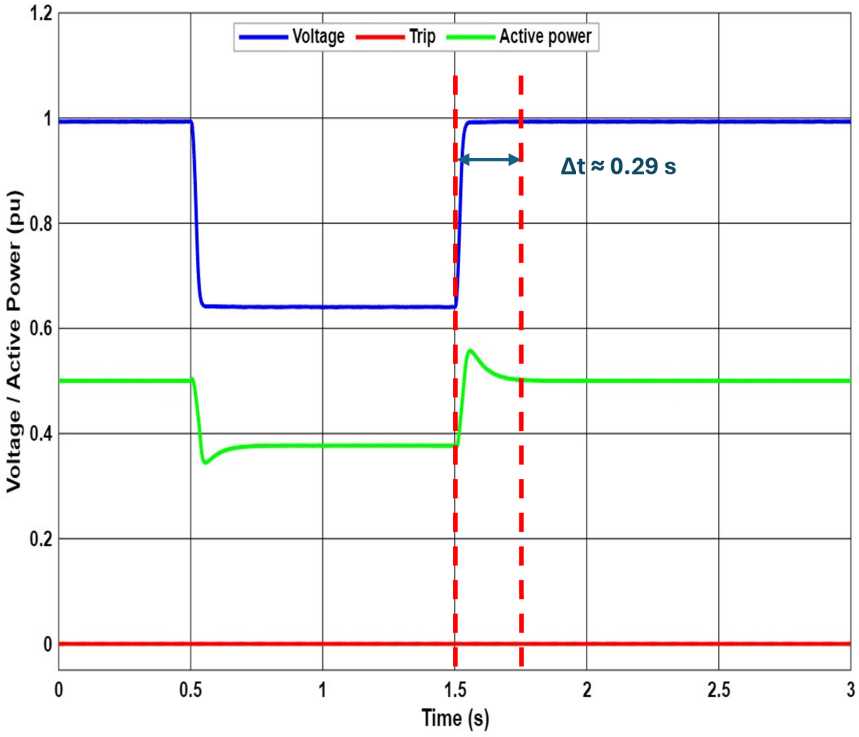

Figure 12. Scenario 5: active power recovery.

In addition to the stay-connected requirement, EN 50549-2 clause 4.5.3.2 mandates that following the return of the terminal voltage to the continuous operating range (above 0.9 p.u.), the FMU must restore at least 90% of its pre-fault active power as fast as technically feasible, and no later than $1\,\mathrm{s}$ after voltage recovery. This requirement was evaluated in Test Case 5, shown in Figure 12, where the voltage was restored to 1.0 p.u. after a $1\,\mathrm{s}$ dip to 0.65 p.u. The simulation results show that the FMU restored its active power

output to its pre-fault level in $0.2\,\mathrm{s}$, which is less than $1\,\mathrm{s}$ from the instant of voltage recovery, satisfying the EN 50549-2 post-fault power recovery requirement.

This result, combined with the ride-through compliance demonstrated previously, confirms that the Danfoss FMU inverter model satisfies all aspects of the EN 50549-2 UVRT requirement.

5.2 OVRT Results

Four test scenarios were executed to evaluate the FMU's over-voltage ride-through behaviour across the full voltage-time compliance boundary that is exactly similar to the one defined in EN 50549-2 clause 4.5.4 for non-synchronous generating technology. In each case seen in Figure 13, three signals are recorded simultaneously: the measured terminal voltage in per unit, the EN 50549-2 OVRT boundary curve evaluated at the current time instant, and the FMU trip signal. Compliance requires the trip signal to remain de-asserted (logic 0) for the entire duration that the voltage-time operating point lies below the boundary curve, and to assert (logic 1) once the operating point crosses into Area C above the boundary.

The first scenario applied a voltage increase (to 1.05 pu) that remained below 1.1 p.u., placing the operating point within the EN 50549-2 continuous operating voltage range defined in clause 4.4.4. No ride-through event was triggered and the trip signal remained at logic 0 throughout, confirming that the FMU does not issue any spurious trips under moderate overvoltage conditions within the normal operating band.

In the second scenario, the voltage was increased to approximately 1.12 p.u., where the FMU is required to remain connected for up to $3\,\mathrm{s}$. The FMU remained connected with the trip signal at logic 0 for $3\,\mathrm{s}$, satisfying this minimum requirement. Once the $3\,\mathrm{s}$ limit was exceeded and the operating point crossed into Area C above the OVRT boundary, the

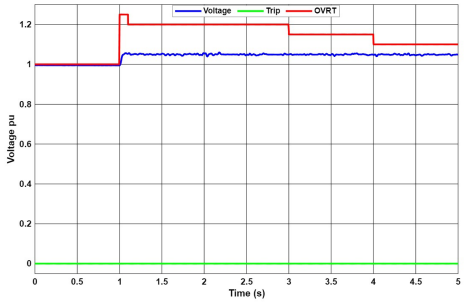

(a) Scenario 1: Voltage increase to 1.05 p.u.

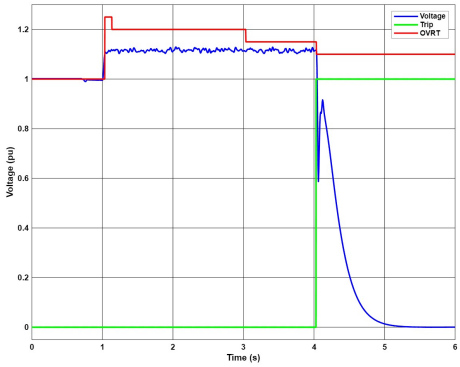

(b) Scenario 2: Voltage swell to 1.12 p.u.

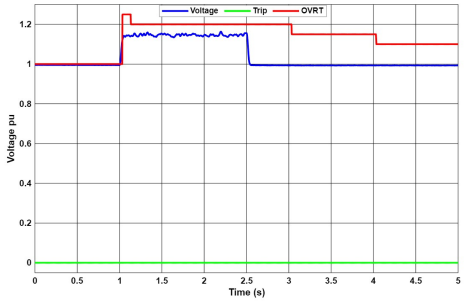

(c) Scenario 3: Voltage swell to 1.15 p.u. for $1.5\,\mathrm{s}$.

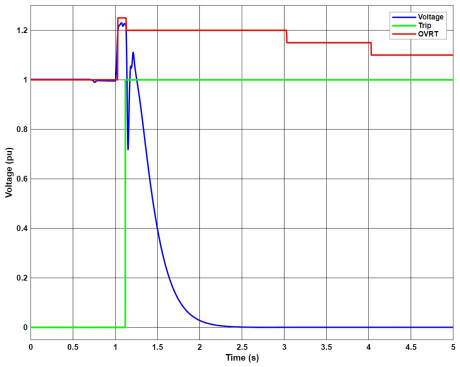

(d) Scenario 4: Voltage swell to 1.22 p.u.

Figure 13. OVRT Compliance Verification.

FMU correctly asserted the trip signal, confirming that the disconnection was both timely and compliant.

The third scenario increased the voltage to 1.15 p.u. and held it for $1.5\,\mathrm{s}$. According to the OVRT stepped boundary, 1.15 p.u. falls within Area B, where the inverter must remain connected for durations up to approximately $2\,\mathrm{s}$ before a trip is permissible. Since the applied duration of $1.5\,\mathrm{s}$ is shorter than the $2\,\mathrm{s}$ minimum threshold at this voltage level, the operating point remained below the OVRT boundary for the entire event. The FMU remained connected with no trip asserted throughout, confirming correct ride-through behaviour in the mid-level overvoltage region.

The fourth scenario applied the most severe test, increasing the voltage to 1.22 p.u. At this level, the FMU is required to remain connected for at least $0.1\,\mathrm{s}$ before a trip is permissible. The FMU remained connected for exactly $0.1\,\mathrm{s}$, satisfying the minimum stay-connected requirement, before the operating point exceeded the OVRT boundary and the trip signal was correctly asserted, demonstrating compliant behaviour under the most extreme short-duration overvoltage condition.

The results across all four scenarios are summarised in Table 13.

Table 13. OVRT Compliance Test Results Summary.

Test Case	Voltage Level	Duration Applied	Min. Required time	Trip Behaviour	Result
1	< 1.1 p.u.	$4\,\mathrm{s}$	Continuous operation	No trip (below boundary)	PASS
2	≈ 1.12 p.u.	$> 3\,\mathrm{s}$	$\approx 3\,\mathrm{s}$	Trip at $3\,\mathrm{s}$ (entered Area C)	PASS
3	1.15 p.u.	$1.5\,\mathrm{s}$ ($<$ required)	$\approx 2\,\mathrm{s}$	No trip (below boundary throughout)	PASS
4	1.22 p.u.	$> 0.1\,\mathrm{s}$	$0.1\,\mathrm{s}$	Trip at $0.1\,\mathrm{s}$ (entered Area C)	PASS

All four scenarios produced a passing result. Test cases 2 and 4 demonstrate that the FMU correctly remains connected for at least the minimum required duration before tripping upon entry into Area C, while test cases 1 and 3 confirm that no spurious tripping occurs when the voltage-time operating point remains below the OVRT boundary curve.

5.3 Frequency Ride-Through Results

Six test scenarios were executed to evaluate the FMU's frequency ride-through behaviour across the full range of under-frequency (UF) and over-frequency (OF) zones defined in EN 50549-2 clause 4.4.2. The three under-frequency scenarios cover each of the sub-nominal frequency bands in descending severity, while the three over-frequency scenarios mirror this structure above the nominal $50\,\mathrm{Hz}$ range. In each case, the measured frequency and the FMU trip signal throughout the simulation are recorded. Compliance requires the trip signal to remain de-asserted (logic 0) for at least the EN 50549-2 minimum stay-connected duration within each frequency band, and to assert (logic 1) only after this minimum duration has been satisfied.

5.3.1 Under-Frequency Results

The three under-frequency scenarios exercise progressively less severe frequency depressions, moving from the outermost band inward toward the nominal range.

In the first scenario Figure 14a, the frequency was reduced to $47.2\,\mathrm{Hz}$, placing the operating point in the $47.0\,\mathrm{Hz}$–$47.5\,\mathrm{Hz}$ band, for which EN 50549-2 carries no mandatory minimum connection time but the simulation time required is $1\,\mathrm{s}$. The FMU remained connected for $1\,\mathrm{s}$, the simulation time allocated for this zone, confirming that the inverter handles the extreme under-frequency band correctly without any uncontrolled response.

In the second scenario 14c, the frequency was reduced to $48.0\,\mathrm{Hz}$, placing the operating point in the $47.5\,\mathrm{Hz}$–$48.5\,\mathrm{Hz}$ band, where a minimum stay-connected duration of $2\,\mathrm{s}$ is required. The simulation was run for $2\,\mathrm{s}$ as the representative test duration for this zone. The FMU remained connected with the trip signal at logic 0 for the full $2\,\mathrm{s}$ simulation period, confirming that the inverter shows no tendency to disconnect prematurely within this band.

In the third scenario 14e, the frequency was reduced to $48.7\,\mathrm{Hz}$, placing the operating point in the $48.5\,\mathrm{Hz}$–$49.0\,\mathrm{Hz}$ band, which also carries a $3\,\mathrm{s}$ minimum requirement. The FMU remained connected for the full $3\,\mathrm{s}$ simulation period allocated for this zone before tripping at the end of the run, again confirming stable ride-through behaviour with no spurious disconnection within the band.

5.3.2 Over-Frequency Results

The three over-frequency scenarios exercise progressively more severe frequency elevations above the nominal range.

In the fourth scenario, the frequency was increased to $50.7\,\mathrm{Hz}$, placing the operating

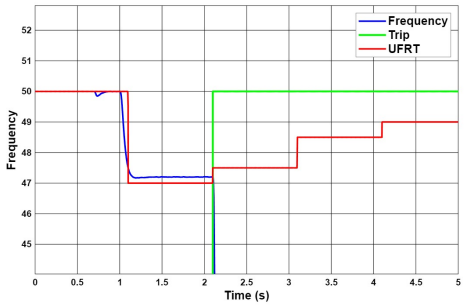

(a) Scenario 1 (UF): Frequency reduced to $47.2\,\mathrm{Hz}$.

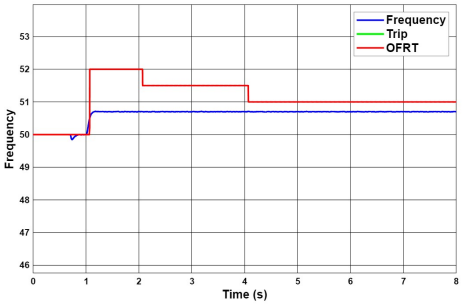

(b) Scenario 4 (OF): Frequency increased to $50.7\,\mathrm{Hz}$.

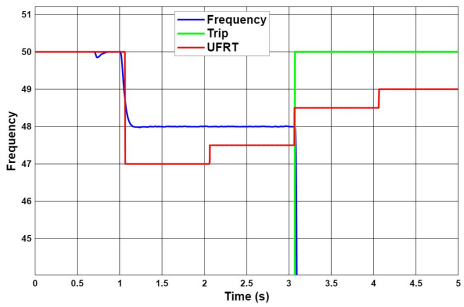

(c) Scenario 2 (UF): Frequency reduced to $48.0\,\mathrm{Hz}$.

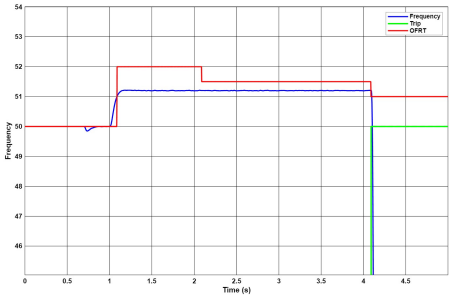

(d) Scenario 5 (OF): Frequency increased to $51.2\,\mathrm{Hz}$.

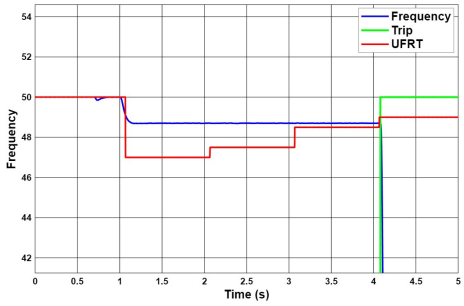

(e) Scenario 3 (UF): Frequency reduced to $48.7\,\mathrm{Hz}$.

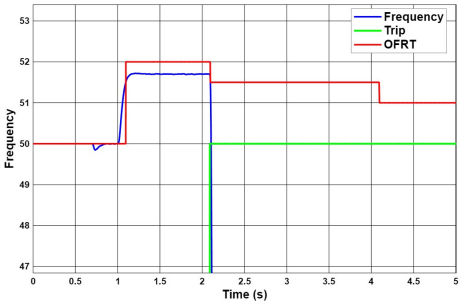

(f) Scenario 6 (OF): Frequency increased to $51.7\,\mathrm{Hz}$.

Figure 14. Frequency Ride-Through Compliance Verification.

point in the $49.0\,\mathrm{Hz}$–$51.0\,\mathrm{Hz}$ nominal band where EN 50549-2 requires unlimited continuous connection. The FMU remained connected for the entire simulation duration, confirming that the inverter correctly identifies this condition as normal operation and issues no trip under any circumstances within the nominal band.

In the fifth scenario, the frequency was increased to $51.2\,\mathrm{Hz}$, placing the operating point in the $51.0\,\mathrm{Hz}$–$51.5\,\mathrm{Hz}$ band, where a minimum stay-connected duration of $3\,\mathrm{s}$ is required. The FMU remained connected for the full $3\,\mathrm{s}$ period, demonstrating compliant ride-through behaviour with no premature disconnection.

In the sixth scenario, the frequency was increased to $51.7\,\mathrm{Hz}$, placing the operating point in the $51.5\,\mathrm{Hz}$–$52.0\,\mathrm{Hz}$ band for which $1\,\mathrm{s}$ is the mandatory minimum connection time. The FMU remained connected for $1\,\mathrm{s}$, confirming correct and controlled behaviour at the upper boundary of the frequency operating range, symmetric with the result observed at $47.2\,\mathrm{Hz}$ in the extreme under-frequency zone.

The results across all six scenarios are summarised in Table 14.

Table 14. Frequency Ride-Through Compliance Test Results Summary.

Scenario	Frequency	Band	EN 50549-2 Min. Required	Simulation requirements	Trip Behaviour	Result
1	$47.2\,\mathrm{Hz}$	$47.0\,\mathrm{Hz}$–$47.5\,\mathrm{Hz}$	Not required	$1\,\mathrm{s}$	after $1\,\mathrm{s}$	PASS
2	$48.0\,\mathrm{Hz}$	$47.5\,\mathrm{Hz}$–$48.5\,\mathrm{Hz}$	$30\,\mathrm{min}$	$2\,\mathrm{s}$	after $2\,\mathrm{s}$	PASS
3	$48.7\,\mathrm{Hz}$	$48.5\,\mathrm{Hz}$–$49.0\,\mathrm{Hz}$	$30\,\mathrm{min}$	$3\,\mathrm{s}$	after $3\,\mathrm{s}$	PASS
4	$50.7\,\mathrm{Hz}$	$49.0\,\mathrm{Hz}$–$51.0\,\mathrm{Hz}$	Unlimited	Unlimited	No trip	PASS
5	$51.2\,\mathrm{Hz}$	$51.0\,\mathrm{Hz}$–$51.5\,\mathrm{Hz}$	$30\,\mathrm{min}$	$3\,\mathrm{s}$	after $3\,\mathrm{s}$	PASS
6	$51.7\,\mathrm{Hz}$	$51.5\,\mathrm{Hz}$–$52.0\,\mathrm{Hz}$	Not required	$1\,\mathrm{s}$	after $1\,\mathrm{s}$	PASS

All six scenarios produced a passing result, confirming that the Danfoss FMU inverter model demonstrates full EN 50549-2 frequency ride-through compliance across all defined under-frequency and over-frequency bands. The FMU exhibited no spurious tripping within any band before its minimum required duration was reached.

5.4 ROCOF Immunity Result

The Rate of Change of Frequency (ROCOF) immunity test was conducted to verify that the FMU remains connected to the distribution network when subjected to frequency ramp rates up to the EN 50549-2 minimum immunity threshold, in compliance with clause 4.5.2. For non-synchronous generating technology, EN 50549-2 clause 4.5.2 mandates a minimum ROCOF immunity of $2\,\mathrm{Hz/s}$, evaluated with a sliding measurement window of

$500\,\mathrm{ms}$.

The test was conducted by applying a linear frequency ramp on the grid emulator side with a rate of $2\,\mathrm{Hz}$ over $1\,\mathrm{s}$, producing a sustained ROCOF of $2\,\mathrm{Hz/s}$ at the point of connection. As shown in Figure 15, the measured ROCOF (blue trace) rises gradually from zero starting at approximately $t = 0.5\,\mathrm{s}$ and reaches the $2\,\mathrm{Hz/s}$ immunity limit (red horizontal line) at approximately $t = 1.57\,\mathrm{s}$. The FMU trip signal (green trace) remained de-asserted at logic 0 throughout the entire ramp period, confirming that the inverter stayed connected for as long as the ROCOF remained below or at the $2\,\mathrm{Hz/s}$ threshold. The trip signal asserted to logic 1 precisely at the instant the measured ROCOF reached the configured $2\,\mathrm{Hz/s}$ limit.

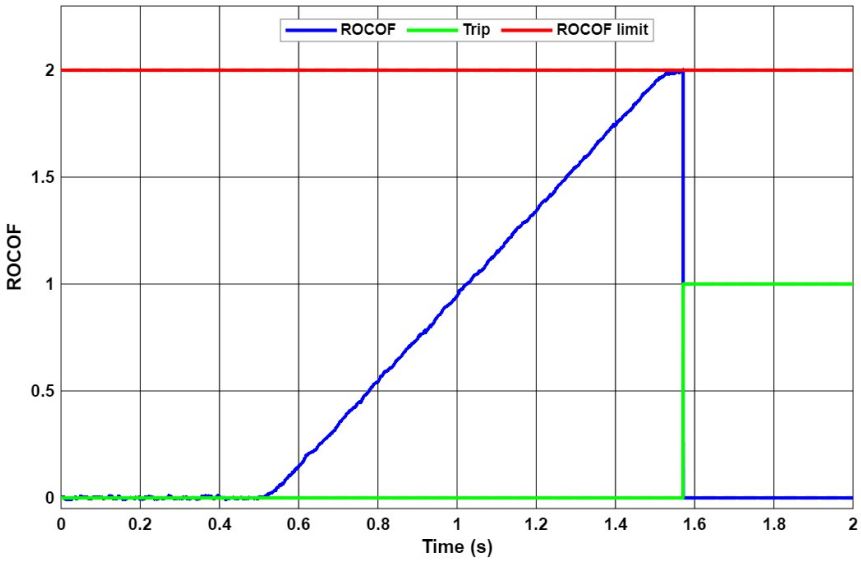

Figure 15. ROCOF Immunity Verification.

5.5 Active Power Response to Frequency Deviation — LFSM-O and LFSM-U Results

The active power frequency response was evaluated across ten test scenarios, one threshold verification test for LFSM-U and LFSM-O and four scenarios each also, to assess the

FMU's compliance with EN 50549-2 clauses 4.6.1 and 4.6.2. All tests were conducted with a configured droop of $s = 5\%$, an intentional delay of $0\,\mathrm{s}$, and reference powers of $P_{\text{ref}} = P_M = 0.5$ p.u. for LFSM-O and $P_{\text{ref}} = P_{\max} = 1.0$ p.u. for LFSM-U, as shown in Table 10. The EN 50549-2 accuracy requirement specifies that the measured active power response must remain within $\pm 10\%$ of nominal power P_n relative to the droop-calculated target value, evaluated as a 1-minute average.

5.5.1 Threshold Verification

Before the droop response scenarios, a baseline test confirmed that no active power change occurred when the frequency remained below the LFSM-O activation threshold of $f_1 = 50.2\,\mathrm{Hz}$ and above the LFSM-U activation threshold of $f_1 = 49.8\,\mathrm{Hz}$. The FMU maintained its pre-disturbance active power setpoint without any frequency-driven adjustment, confirming that the LFSM functions are correctly gated by their respective threshold conditions and do not interact with normal operating frequency variations within the continuous operating band as shown in Figure 16.

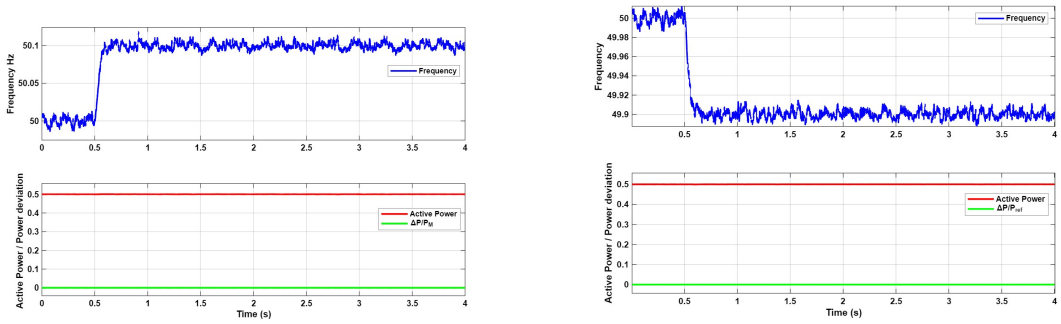

(a) LFSM-O Threshold Verification.

(b) LFSM-U Threshold Verification.

Figure 16. LFSM Activation Threshold Verification.

5.5.2 LFSM-U Results

Four under-frequency test points were applied by stepping the grid emulator frequency to $49.6\,\mathrm{Hz}$, $49.4\,\mathrm{Hz}$, $49.2\,\mathrm{Hz}$, and $49.0\,\mathrm{Hz}$, each representing a progressively deeper under-

frequency deviation below the $f_1 = 49.8\,\mathrm{Hz}$ activation threshold. For each operating point, the expected active power increase $\Delta P/P_{\text{ref}}$ was computed from the droop equation 4:

$$\frac{\Delta P}{P_{\text{ref}}} = \frac{f_1 - f}{s \cdot f_n} = \frac{49.8 - f}{0.05 \times 50} \tag{4}$$

The most demanding test point at $49.0\,\mathrm{Hz}$ yields a theoretical $\Delta P/P_{\text{ref}}$ of +32%, corresponding to a target active power increase to $P_M + 0.32 \times P_{max} = 0.5 + 0.32 = 0.82$ p.u. as per equation 2. The simulation produced a measured active power deviation of 31.98% as seen in figure 18b, deviating from the target by only 0.02 percentage points, well within the $\pm 10\%\, P_n$ tolerance band. The results for all four under-frequency test points, together with the $\pm 10\%\, P_n$ tolerance band boundaries, are presented in Figure 17b, confirming that all operating points lie within the EN 50549-2 accuracy envelope and Table 15 summarize these four test cases with there numerical values.

Table 15. LFSM-U Active Power Response Accuracy Summary.

Frequency	**Theoretical** $\Delta P/P_{\text{ref}}$	**Simulated** $\Delta P/P_{\text{ref}}$	**Within** $\pm 10\%\, P_n$
$49.6\,\mathrm{Hz}$	$+8.00\%$	$+8.07\%$	Yes
$49.4\,\mathrm{Hz}$	$+16.00\%$	$+16.10\%$	Yes
$49.2\,\mathrm{Hz}$	$+24.00\%$	$+24.12\%$	Yes
$49.0\,\mathrm{Hz}$	$+32.00\%$	$+31.98\%$	Yes

5.5.3 LFSM-O Results

Four over-frequency test points were applied by stepping the grid emulator frequency to $50.4\,\mathrm{Hz}$, $50.6\,\mathrm{Hz}$, $50.8\,\mathrm{Hz}$, and $51.0\,\mathrm{Hz}$, each representing a progressively deeper over-frequency deviation above the $f_1 = 50.2\,\mathrm{Hz}$ activation threshold. The expected active power reduction at each point was computed from the droop equation 5:

$$\frac{\Delta P}{P_{\text{ref}}} = \frac{f_1 - f}{s \cdot f_n} = \frac{50.2 - f}{0.05 \times 50} \tag{5}$$

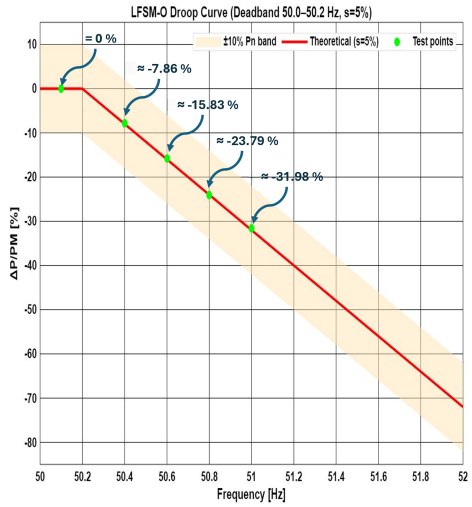

(a) LFSM-O Test Points.

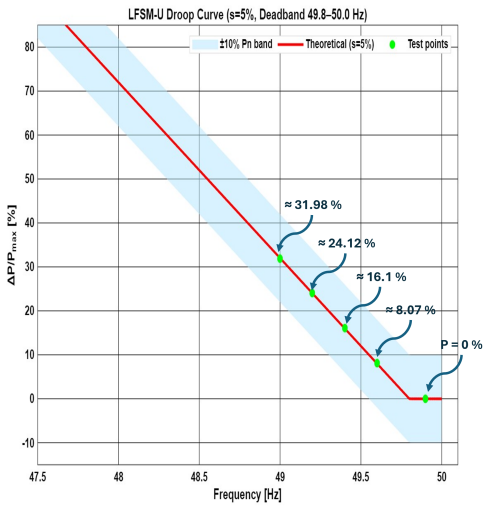

(b) LFSM-U Test Points.

Figure 17. LFSM Accuracy Limit Verification.

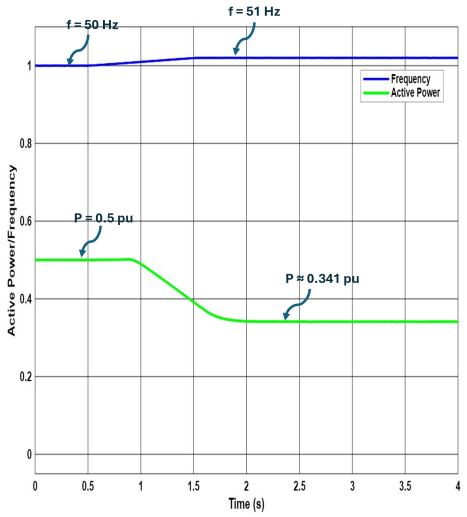

(a) LFSM-O Active Power Response.

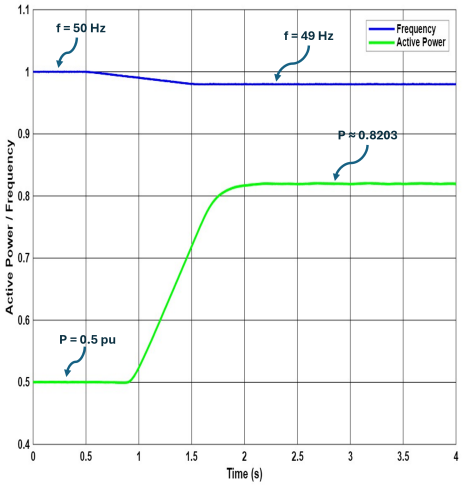

(b) LFSM-U Active Power Response.

Figure 18. LFSM Active Power Response.

The most demanding test point at $51.0\,\mathrm{Hz}$ yields a theoretical $\Delta P/P_{\text{ref}}$ of -32%, corresponding to a target active power of $P_M \times (1 - 0.32) = 0.5 \times 0.68 = 0.34$ p.u. The simulation produced a measured active power of 0.341 p.u. as seen in figure 18a, deviating from the target by only 0.001 p.u., well within the $\pm 10\%\, P_n$ tolerance band. The measured $\Delta P/P_{\text{ref}}$ at this point was -31.98% against the theoretical -32%, representing an error of 0.22 percentage points. The results for all four over-frequency test points are

presented in Figure 17a alongside the $\pm 10\%\ P_n$ tolerance band, confirming that all points remain within the EN 50549-2 accuracy envelope and the Table 16 summarize these four test cases with there numerical values.

Table 16. LFSM-O Active Power Response Accuracy Summary.

Frequency	**Theoretical** $\Delta P/P_{\text{ref}}$	**Simulated** $\Delta P/P_{\text{ref}}$	**Within** $\pm 10\%\ P_n$
$50.4\,\text{Hz}$	-8.00%	-7.86%	Yes
$50.6\,\text{Hz}$	-16.00%	-15.83%	Yes
$50.8\,\text{Hz}$	-24.00%	-23.79%	Yes
$51.0\,\text{Hz}$	-32.00%	-31.98%	Yes

All ten test scenarios, the threshold verifications, four LFSM-U points, and four LFSM-O points, produced results consistent with the EN 50549-2 active power frequency response requirements. The maximum observed deviation across all eight droop test points was less than 0.25 percentage points from the theoretical $\Delta P/P_{\text{ref}}$ value, confirming that the FMU's frequency-to-power droop characteristic is accurately implemented and that all simulated operating points lie comfortably within the $\pm 10\%\ P_n$ accuracy band specified in EN 50549-2 clauses 4.6.1 and 4.6.2.

5.5.4 Dead Time and Step Response Time Verification

In addition to the droop accuracy tests, the dynamic response characteristics of the LFSM-O and LFSM-U functions were verified against the EN 50549-2 requirements, which specify a maximum dead time of $2\,\text{s}$ and a maximum step response time of $30\,\text{s}$. Both parameters were evaluated from a single test in which a step frequency change was applied simultaneously in both the over-frequency and under-frequency directions, with the active power response recorded at high time resolution.

The results, presented in Figure 19, show that the FMU began responding in the right way to the frequency step in $0.2\,\text{s}$ in both the LFSM-O and LFSM-U directions, well within the $2\,\text{s}$ maximum dead time permitted by EN 50549-2. This fast dead time is consistent with the inverter-based architecture of the FMU, which does not involve any mechani-

cal inertia or slow thermal process that would introduce an inherent delay in the power control loop. Furthermore, the FMU reached its droop-calculated active power target value within $1\,\mathrm{s}$ of the frequency step, satisfying the $30\,\mathrm{s}$ maximum step response time requirement by a substantial margin. The combination of a $0.2\,\mathrm{s}$ dead time and a $1\,\mathrm{s}$ step response time confirms that the FMU's active power frequency response is significantly faster than the EN 50549-2 minimum dynamic performance thresholds in both frequency deviation directions.

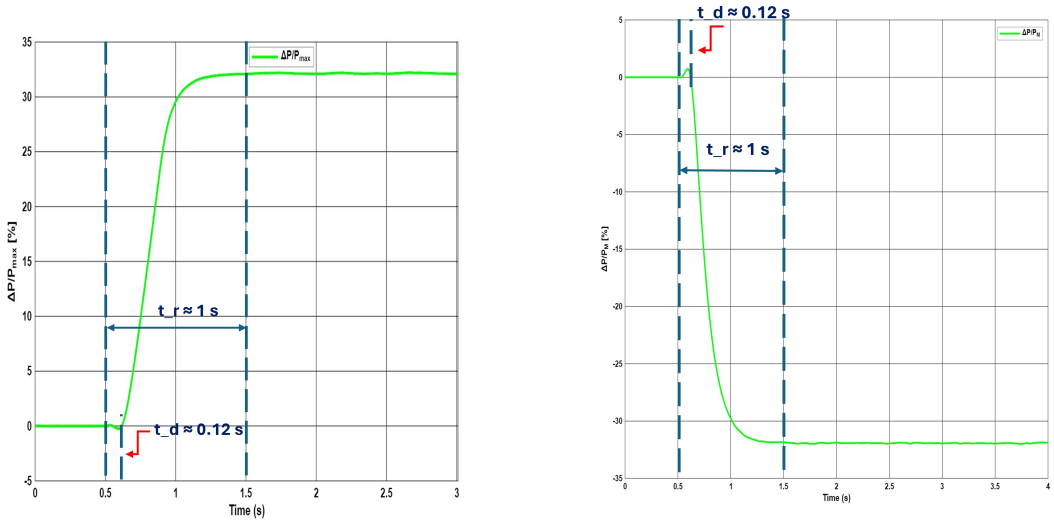

(a) LFSM-U Dynamic Response.

(b) LFSM-O Dynamic Response.

Figure 19. LFSM Dynamic Performance Verification for dead time and step response time.

5.5.5 Frequency Measurement Resolution Verification

The EN 50549-2 requires the frequency measurement resolution of the generating plant to be $10\,\mathrm{mHz}$ or less, ensuring that small frequency deviations just above the activation threshold f_1 are detected and acted upon correctly. To verify this, a dedicated resolution test was conducted in which the grid emulator applied a frequency deviation of exactly $\pm 10\,\mathrm{mHz}$ relative to the respective activation thresholds. Based on the droop equation with $s = 5\%$ and $f_n = 50\,\mathrm{Hz}$, a $10\,\mathrm{mHz}$ frequency deviation produces a theoretical active power change of:

$$\frac{\Delta P}{P_{\text{ref}}} = \frac{0.01}{0.05 \times 50} = 0.4\% \tag{6}$$

The simulation results showed in Figure 20 confirmed that the FMU detected the $\pm 10\,\text{mHz}$ frequency deviation and produced a measurable active power change of $0.4\%\,\Delta P/P_{\text{ref}}$ in both the LFSM-O and LFSM-U directions, consistent with the theoretical expectation. This confirms that the FMU's internal frequency measurement chain achieves the required $10\,\text{mHz}$ resolution and that the droop control responds correctly to the smallest frequency deviation mandated by EN 50549-2, without missing or filtering out sub-threshold variations at the activation boundary.

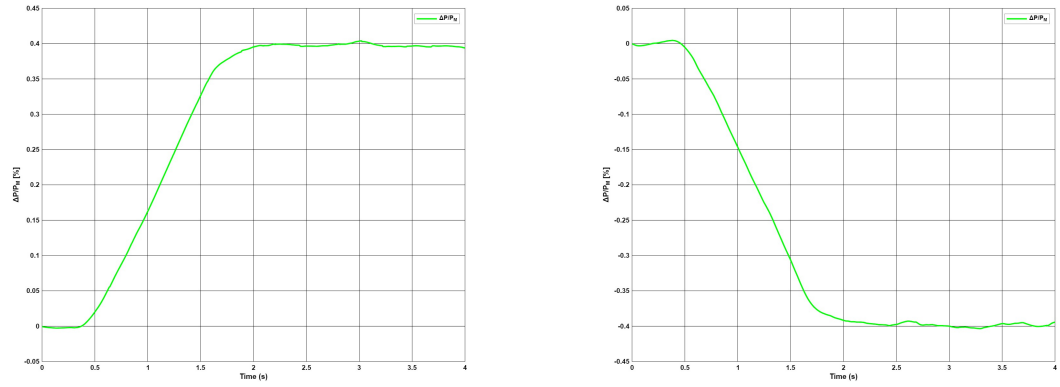

(a) LFSM-U Resolution Test.

(b) LFSM-O Resolution Test.

Figure 20. Frequency Measurement Resolution Verification.

5.6 Voltage Support by Reactive Power — Q(U) Results

The steady-state accuracy of the Q(U) volt-var characteristic was evaluated across ten test points spanning the full operating range of the configured curve shown in Figure 10, covering both the over-excited (under-voltage) and under-excited (over-voltage) reactive power regions. For each test point, the grid emulator held the terminal voltage at a fixed per-unit level and the measured reactive power output once steady state was reached is recorded. The EN 50549-2 static accuracy requirement specifies that the reactive power

shall be delivered with an accuracy of $\pm 2\%\, S_{\max}$ when the generating plant is operating above the apparent power threshold $S_{\min} = 10\%\, S_{\max}$. The configured Q(U) characteristic has a deadband between 97% and $103\%\, U_n$, maximum reactive power limits of $\pm 33\%\, P_D$ on both sides, and a slope of $5\%/\%$ outside the deadband.

Ten voltage operating points were applied, ranging from 80% to $115\%\, U_n$, covering both the deadband region and the full reactive power delivery range on both sides of the characteristic. The measured reactive power deviation ΔQ at each test point is presented in Table 17, and all ten points are plotted on the configured Q(U) characteristic curve in Figure 23, together with the $\pm 2\%\, S_{\max}$ static accuracy tolerance band.

Test points 5 and 6 fall within the configured deadband (97%–$103\%\, U_n$) and correctly produce zero reactive power output change, confirming that the inverter does not inject reactive power unnecessarily during normal voltage conditions as shown in Figure 21.

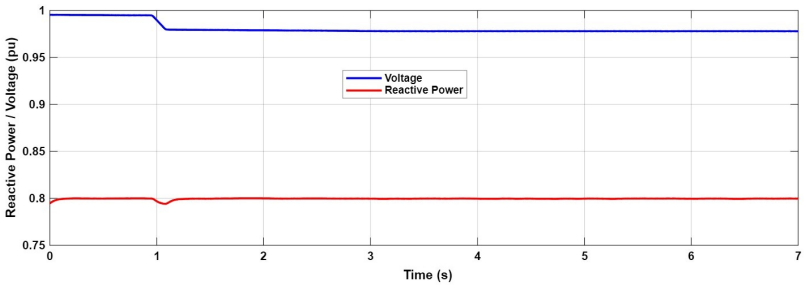

(a) Deadband Verification (UV).

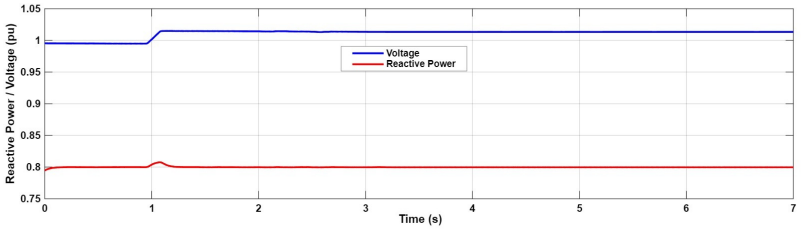

(b) Deadband Verification (OV).

Figure 21. Q(U) Deadband Verification.

Four points were selected for detailed waveform analysis as shown in Figure 22, with individual figures showing the time-domain evolution of terminal voltage, reactive power output, and ΔQ for each case. The four selected operating points span both the under-voltage (capacitive) and over-voltage (inductive) regions of the $Q(U)$ characteristic defined by Eq. 3.

Point at $93\%\, U_n$: Falls in the linear under-voltage droop region. The theoretical value of $+20.00\%$ is computed directly from $5(97-93)\%$. The simulated value of $+20.58\%$ shows a small positive overshoot of 0.58 percentage points, consistent with transient reactive current injection dynamics.

Point at $80\%\, U_n$: Well below the 90.4% saturation threshold, so the characteristic is clamped at $+33.00\%$. The FMU matches this exactly, confirming correct saturation behavior.

Point at $108\%\, U_n$: Falls in the linear over-voltage droop region. The theoretical value of -25.00% is computed from $-5(108-103)\%$. The simulated value of -25.70% deviates by 0.70 percentage points.

Point at $115\%\, U_n$: Above the 109.6% saturation threshold, so the characteristic is clamped at -33.00%. The simulated value of -32.70% shows a slight under-delivery of 0.30 percentage points, still well within acceptable tolerance.

Note for Figure 22 Clarification: In steady-state operation, the inverter absorbs reactive power from the grid. Consequently, during under-voltage events, the injected reactive current acts in opposition to the pre-fault operating point, causing the net measured reactive power to decrease; however, this correctly reflects positive ΔQ injection per the $Q(U)$ characteristic. Conversely, during over-voltage events, the absorbed reactive power aligns with the steady-state direction, increasing the total reactive power magnitude, which equally represents correct inductive absorption behavior.

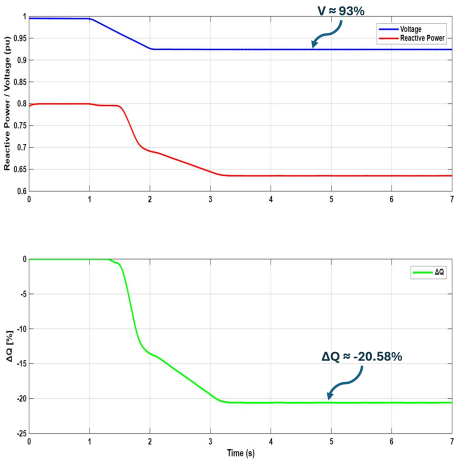

(a) Mid-Slope Under-Voltage: $U = 93\%\, U_n$. Measured $\Delta Q = 20.58\%\, P_D$ injected.

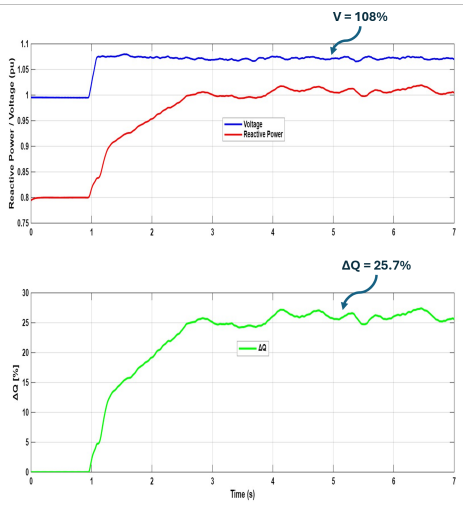

(b) Mid-Slope Over-Voltage: $U = 108\%\, U_n$. Measured $\Delta Q = 25.70\%\, P_D$ absorbed.

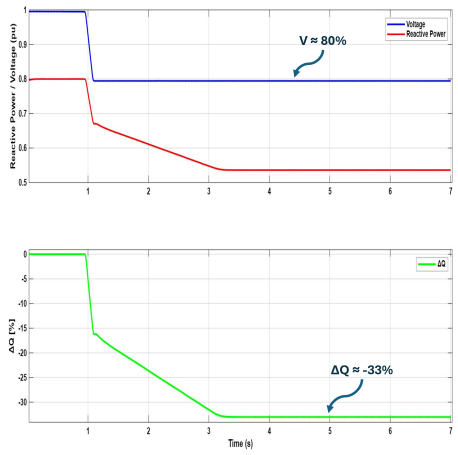

(c) Max Under-Voltage Injection: $U = 80\%\, U_n$. Measured $\Delta Q = 33.0\%\, P_D$ injected.

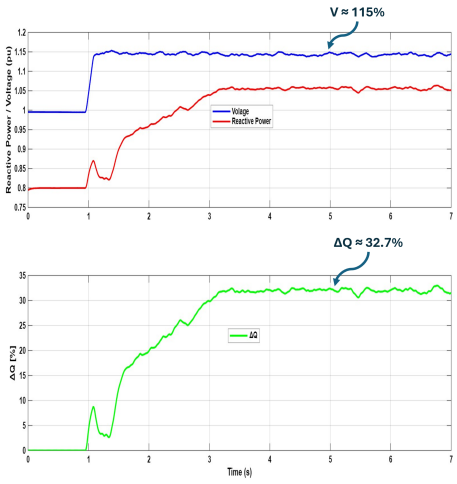

(d) Max Over-Voltage Absorption: $U = 115\%\, U_n$. Measured $\Delta Q = 32.70\%\, P_D$ absorbed.

Figure 22. Q(U) Waveform Analysis.

All ten steady-state test points and all four detailed waveform cases produced results consistent with EN 50549-2 requirements, confirming full Q(U) compliance of the Danfoss FMU inverter model across the entire configured volt-var characteristic.

The dynamic accuracy of the Q(U) control was evaluated by applying step voltage changes into both the over-voltage and under-voltage regions and recording the transient reactive

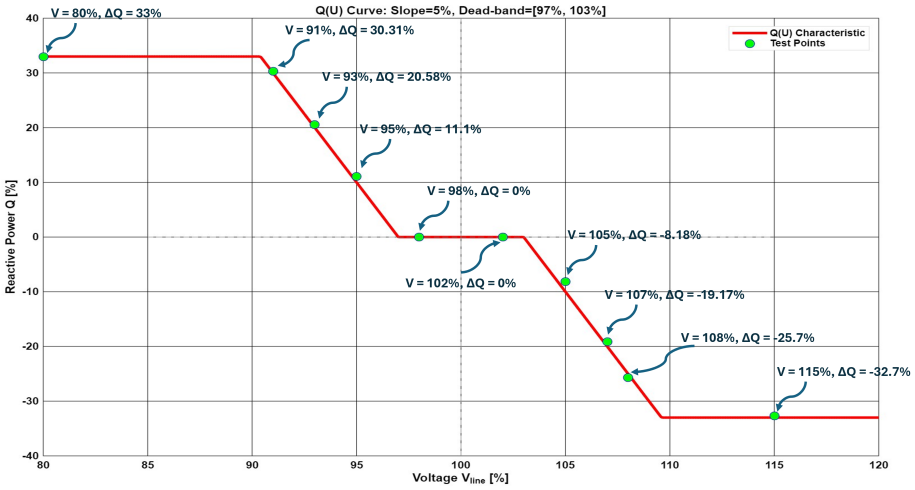

Figure 23. Q(U) Static Accuracy test points.

Table 17. Q(U) Static Accuracy Test Results.

Test Point	Voltage [% U_n]	Theoretical ΔQ [% P_D]	Measured ΔQ [% P_D]
1	80%	$+33.00\%$	$+33.00\%$
2	91%	$+30.00\%$	$+30.31\%$
3	93%	$+20.00\%$	$+20.58\%$
4	95%	$+10.00\%$	$+11.10\%$
5	98%	0%	0%
6	102%	0%	0%
7	105%	-10.00%	-8.18%
8	107%	-20.00%	-19.17%
9	108%	-25.00%	-25.70%
10	115%	-33.00%	-32.70%

power response against the EN 50549-2 dynamic tolerance band. According to EN 50549-2, the Q(U) control dynamics shall correspond to a first-order filter with the configured time constant $T_c = 3\,\mathrm{s}$, within a tolerance of $\pm 5\%\ P_D$ plus a time delay allowance of up to $3\,\mathrm{s}$ relative to the ideal first-order filter trajectory. For a first-order system, the output is expected to reach 63.2% of the step target value after one time constant T_c, and 95% of the target value after approximately three time constants $3 \times T_c = 9\,\mathrm{s}$.

The results for both the over-voltage and under-voltage step cases are presented in Figures 24a and 24b, respectively. In the over-voltage case, the reactive power response reached 63.2% of its target value at $3.14\,\mathrm{s}$, closely matching the configured $T_c = 3\,\mathrm{s}$ and

deviating from the ideal first-order response by only $0.14\,\mathrm{s}$. The 95% target value was reached at $9.035\,\mathrm{s}$, consistent with the theoretical $3T_c = 9\,\mathrm{s}$ expectation and confirming that the full settling behaviour of the control loop accurately follows the configured time constant.

In the under-voltage case, the 63.2% point was reached at $4.2\,\mathrm{s}$, which represents a slightly slower initial response compared to the over-voltage case but remains within the EN 50549-2 dynamic tolerance band that permits deviations of up to $\pm 5\%\ P_D$ plus a $3\,\mathrm{s}$ time delay from the ideal trajectory. In both cases, the reactive power transient remained entirely within the $\pm 5\%\ P_D$ tolerance band throughout the settling period, with no overshoot or oscillation observed beyond the permitted envelope.

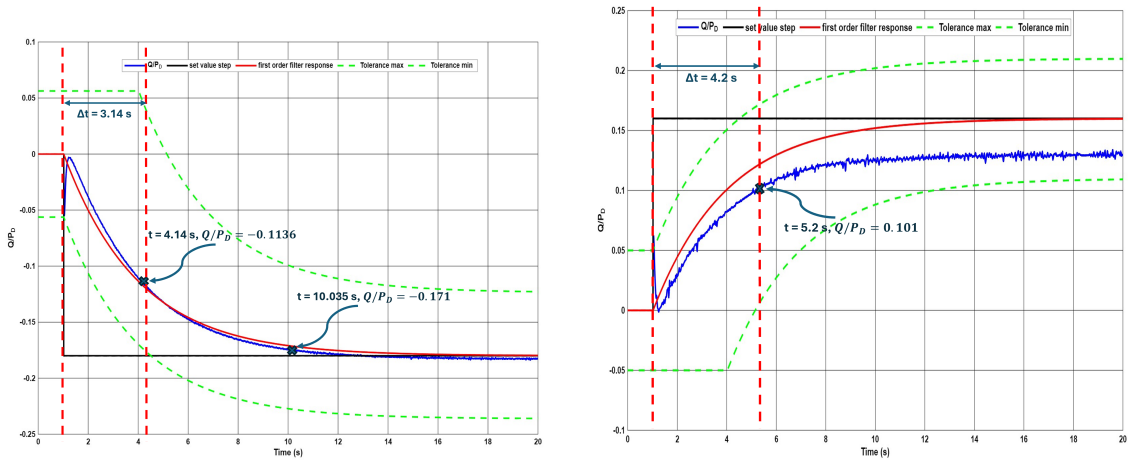

(a) Over-Voltage Step Response.

(b) Under-Voltage Step Response.

Figure 24. Q(U) Dynamic Step Response Verification.

The close agreement between the simulated time constants and the configured $T_c = 3\,\mathrm{s}$ value, combined with full containment within the EN 50549-2 dynamic accuracy band in both the over-voltage and under-voltage directions, confirms that the FMU's Q(U) dynamic response is correctly parameterised and compliant with EN 50549-2.

5.7 Dynamic Reactive Current During Asymmetrical Faults Results

Five asymmetrical fault scenarios were simulated to evaluate the FMU's dynamic reactive current injection capability in compliance with EN 50549-2 clause 4.7.4.2.1. The fault types tested were a Single Line-to-Ground Fault (SLGF), a Double Line Fault (DLF), and a Double Line-to-Ground Fault (DLGF), with three SLGF variants applied at different severity levels. Each fault type produces distinct positive- and negative-sequence voltage deviations ΔV_1 and ΔV_2, which drive the expected additional reactive current injections ΔI_{Q1} and ΔI_{Q2} through the configured gradient $k = 2$. The EN 50549-2 accuracy requirement for the additional reactive current is defined by Figure 18 of the standard, which permits a lower tolerance of $-10\%\, I_r$ and an upper tolerance of $+20\%\, I_r$ in the relevant operating quadrants. For each fault scenario, the measured ΔI_{Q1} and ΔI_{Q2} are compared against their expected values computed from $I_Q = k \cdot \Delta V$, and the resulting errors are evaluated against the EN 50549-2 tolerance band.

The three primary fault scenarios are presented individually in Figures 25, 26, and 27, each showing the time-domain evolution of the positive- and negative-sequence voltages and the corresponding reactive current responses.

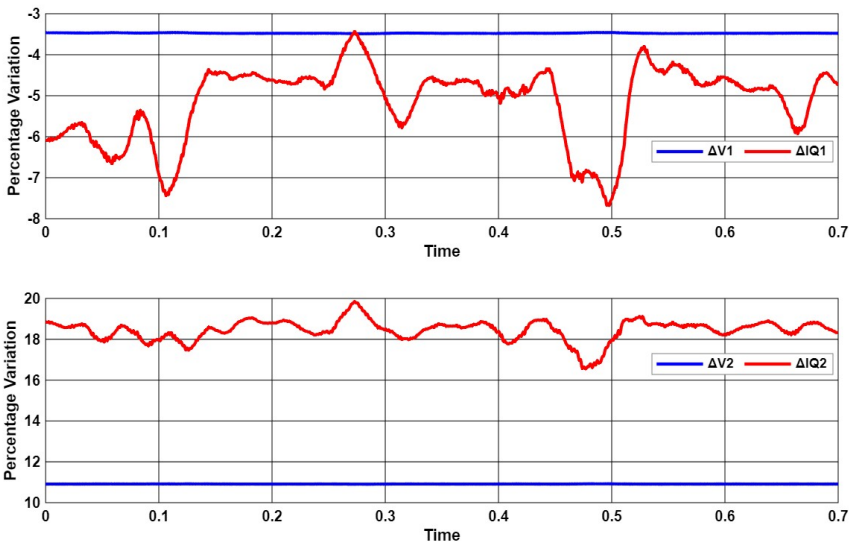

Figure 25. Single Line-to-Ground Fault (SLGF) Response.

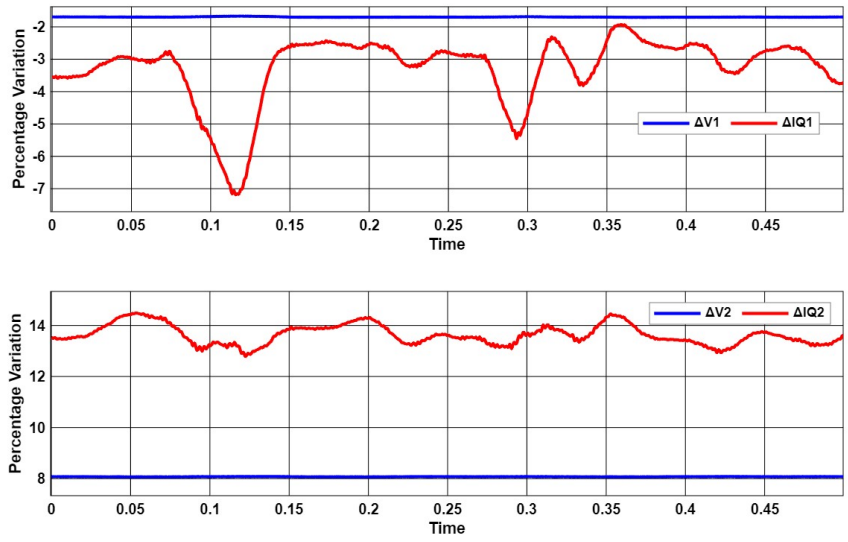

Figure 26. Double Line Fault (DLF) Response.

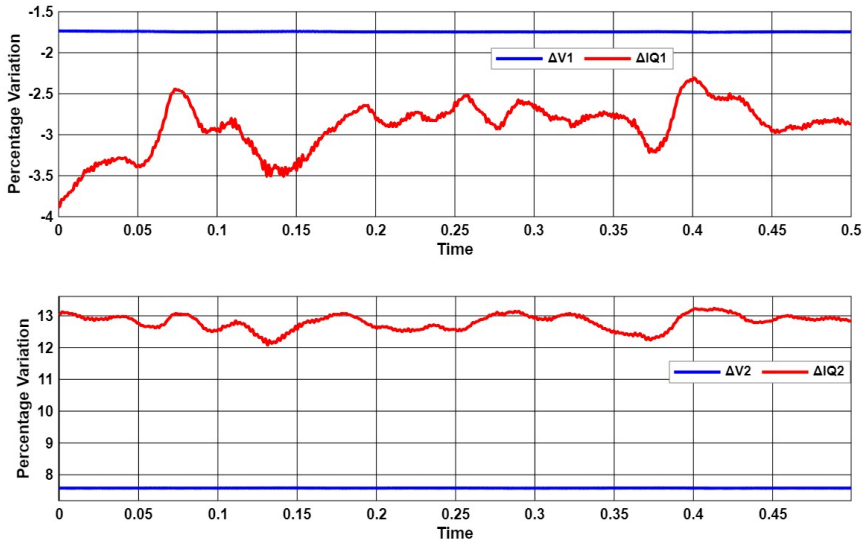

Figure 27. Double Line-to-Ground Fault (DLGF) Response.

In the SLGF case (Figure 25), the fault produced a positive-sequence voltage deviation of $\Delta V_1 = +3.48\%\, U_c$ and a negative-sequence deviation of $\Delta V_2 = +10.91\%\, U_c$. With $k = 2$, the expected reactive current responses are $\Delta I_{Q1} = +6.95\%\, I_r$ and $\Delta I_{Q2} = +21.83\%\, I_r$. The simulation produced $\Delta I_{Q1} = +5.15\%\, I_r$ and $\Delta I_{Q2} = +18.46\%\, I_r$, with errors of $-1.80\%\, I_r$ and $-3.37\%\, I_r$, respectively. Both errors are negative, meaning

the FMU slightly under-delivers relative to the ideal k-factor response, but remain well within the $-10\%\, I_r$ lower tolerance boundary of EN 50549-2 Figure 18.

In the DLF case (Figure 26), the fault produced $\Delta V_1 = -1.70\%\, U_c$ and $\Delta V_2 = +8.08\%\, U_c$. The expected responses are $\Delta I_{Q1} = -3.39\%\, I_r$ and $\Delta I_{Q2} = +16.15\%\, I_r$. The simulation produced $\Delta I_{Q1} = -3.33\%\, I_r$ and $\Delta I_{Q2} = +13.70\%\, I_r$, with errors of $+0.06\%\, I_r$ and $-2.45\%\, I_r$, respectively, both within the EN 50549-2 tolerance band. The near-zero error of $+0.06\%\, I_r$ on the positive-sequence channel confirms particularly accurate tracking of the k-factor gradient for this fault type.

In the DLGF case (Figure 27), the fault produced $\Delta V_1 = -1.74\%\, U_c$ and $\Delta V_2 = +7.58\%\, U_c$. The expected responses are $\Delta I_{Q1} = -3.49\%\, I_r$ and $\Delta I_{Q2} = +15.16\%\, I_r$. The simulation produced $\Delta I_{Q1} = -2.95\%\, I_r$ and $\Delta I_{Q2} = +12.76\%\, I_r$, with errors of $+0.54\%\, I_r$ and $-2.40\%\, I_r$, respectively, both well within the EN 50549-2 tolerance band.

The complete results across all five fault scenarios for both the positive-sequence (ΔI_{Q1}) and negative-sequence (ΔI_{Q2}) reactive current channels are presented in Tables 18 and 19, respectively, and all operating points are plotted collectively in Figure 28 against the EN 50549-2 accuracy tolerance boundaries.

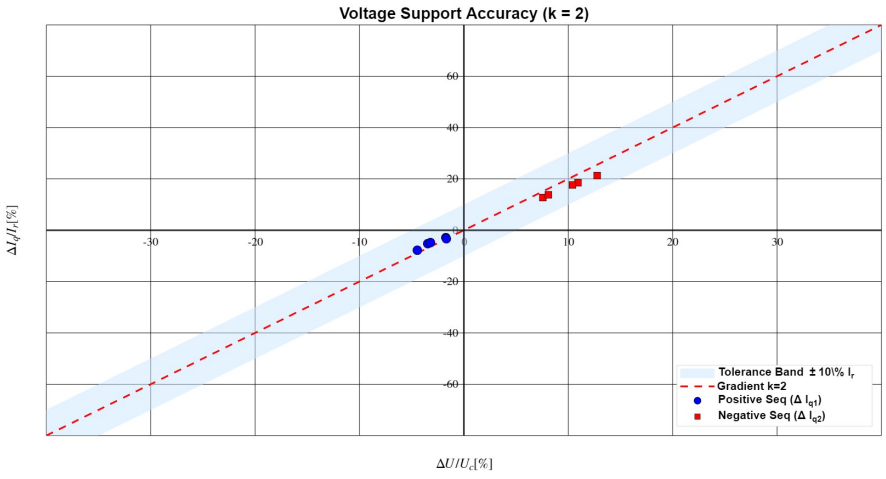

Figure 28. All 5 asymmetrical test cases.

Table 18. Positive-Sequence Reactive Current (ΔI_{Q1}) Accuracy Results.

Case	ΔV_1 [% U_c]	Expected [% I_r]	Measured ΔI_{Q1} [% I_r]	Error [% I_r]	Result
C1 — SLGF	-3.48%	-6.95%	-5.15%	$+1.80\%$	PASS
C2 — SLGF	-3.22%	-6.44%	-4.81%	$+1.63\%$	PASS
C3 — SLGF	-4.47%	-8.94%	-7.79%	$+1.14\%$	PASS
C4 — DLGF	-1.74%	-3.49%	-2.95%	$+0.54\%$	PASS
C5 — DLF	-1.70%	-3.39%	-3.33%	$+0.06\%$	PASS

Table 19. Negative-Sequence Reactive Current (ΔI_{Q2}) Accuracy Results.

Case	ΔV_2 [% U_c]	Expected [% I_r]	Measured ΔI_{Q2} [% I_r]	Error [% I_r]	Result
C1 — SLGF	$+10.91\%$	$+21.83\%$	$+18.46\%$	-3.37%	PASS
C2 — SLGF	$+10.41\%$	$+20.82\%$	$+17.59\%$	-3.23%	PASS
C3 — SLGF	$+12.75\%$	$+25.50\%$	$+21.38\%$	-4.12%	PASS
C4 — DLGF	$+7.58\%$	$+15.16\%$	$+12.76\%$	-2.40%	PASS
C5 — DLF	$+8.08\%$	$+16.15\%$	$+13.70\%$	-2.45%	PASS

All five fault scenarios passed the EN 50549-2 dynamic reactive current accuracy requirement across both the positive- and negative-sequence channels. The errors on the positive-sequence channel ΔI_{Q1} ranged from $+0.06\%$ to $+1.80\%\, I_r$, and the errors on the negative-sequence channel ΔI_{Q2} ranged from -2.40% to $-4.12\%\, I_r$, all remaining well within the EN 50549-2 Figure 18 lower tolerance of $-10\%\, I_r$.

6 Conclusions and Future Work

6.1 Summary of Contributions

This thesis developed and validated a Software-in-the-Loop compliance testing framework for the Danfoss FMU grid-connected inverter, targeting the full set of operational requirements defined in EN 50549-2 for non-synchronous generating plants connected to MV distribution networks. The central contribution is the integration of the FMU binary into a MATLAB/Simulink co-simulation environment alongside a controllable grid emulator, enabling automated real-time evaluation of compliance across different test categories within a single unified framework. Compared to prior work in simulation-based grid code compliance testing, which has predominantly focused on symmetrical fault ride-through and basic frequency response, this thesis extends coverage to include ROCOF immunity, asymmetrical fault reactive current support across three fault types (SLGF, DLF, DLGF), LFSM-O and LFSM-U droop accuracy including dead time and resolution verification, and full Q(U) volt-var characterisation encompassing both steady-state accuracy and dynamic step response.

The simulation results demonstrated full EN 50549-2 compliance across all tested scenarios, with no failures observed in any of the test categories. The UVRT and OVRT boundary tracking was accurate to within the simulation timestep resolution, the LFSM droop errors remained below 0.25 percentage points across all eight frequency test points, the Q(U) steady-state accuracy was within $\pm 2\%\, S_{\max}$ across all ten voltage operating points, and the asymmetrical fault reactive current errors remained within the EN 50549-2 tolerance band across all five fault scenarios. The framework demonstrated that a SIL approach can provide a high-fidelity, repeatable, and computationally efficient alternative to physical pre-certification testing, substantially reducing the time and cost required to identify compliance issues early in the inverter development cycle.

6.2 Future Work

Several extensions to the current framework are identified as high-priority directions for future research and development.

Power Hardware-in-the-Loop (P-HIL) validation: The most immediate next step is to replicate the complete EN 50549-2 test campaign in the FREESI laboratory using the P-HIL infrastructure, where the Danfoss inverter hardware is interfaced with a real-time grid emulator through a power amplifier. This would allow a direct quantitative comparison between the SIL and P-HIL results across all nine test categories, establishing the fidelity limits of the SIL framework and providing the accredited measurement data required for formal type testing submission.

Grid-forming inverter compliance testing: The growing deployment of grid-forming (GFM) inverters in distribution networks introduces compliance requirements, including inertia emulation, virtual synchronous machine behaviour, and black-start capability, that are not addressed in the current EN 50549-2 framework. Extending the framework to evaluate GFM-specific grid code requirements, such as those emerging in Fingrid, AEMO, and VDE FNN, represents a significant research opportunity as the regulatory landscape evolves.

Aggregated plant modelling: The current framework tests a single inverter unit in isolation. Future work should extend the co-simulation environment to model aggregated generating plants comprising multiple FMU instances connected through an internal MV collector network, enabling compliance testing at the plant level and capturing the interaction effects between units, particularly for reactive power sharing under Q(U) mode and sequence current distribution during asymmetrical faults, that are not visible in single-unit testing.

Bibliography

Ahmed, I., Rehan, M., Basit, A., Ahmad, H., Ahmed, W., Ullah, N., ... Prokop, L. (2023). Review on microgrids design and monitoring approaches for sustainable green energy networks. *Scientific Reports*, *13*. Retrieved from https://api.semanticscholar.org/CorpusID:266135737

Ally, C. Z., & de Jong, E. C. W. (2021). Obtaining robust performance of a current fed voltage source inverter for virtual inertia response in a low short circuit ratio condition. *Energies*. Retrieved from https://api.semanticscholar.org/CorpusID:239658471

Almeida, D., Pasupuleti, J., & Ekanayake, J. B. (2021). Comparison of reactive power control techniques for solar pv inverters to mitigate voltage rise in low-voltage grids. *Electronics*. Retrieved from https://api.semanticscholar.org/CorpusID:237790505

Almeida, D., Pasupuleti, J., Raveendran, S. K., & Khan, M. R. B. (2021). Performance evaluation of solar pv inverter controls for overvoltage mitigation in mv distribution networks. *Electronics*. Retrieved from https://api.semanticscholar.org/CorpusID:237865026

Awal, M. A., Cen, S., Rachi, M. R. K., Yu, H., Schröder, S., & Husain, I. (2024). Modeling, analysis, and design for small-signal stability in sequence-decomposed grid-forming control. *IEEE Transactions on Industry Applications*, *60*, 865-875. Retrieved from https://api.semanticscholar.org/CorpusID:264467723

Bai, K., Sindhu, V., & Haque, A. (2023). Fault ride through approach for grid-connected photovoltaic system. *e-Prime - Advances in Electrical Engineering, Electronics and Energy*, *5*, 100232. https://doi.org/https://doi.org/10.1016/j.prime.2023.100232

Brandl, R., Kotsampopoulos, P. C., Lauss, G., Maniatopoulos, M., Nuschke, M., Montoya, J., ... Strauss-Mincu, D. (2018). Advanced testing chain supporting the validation of smart grid systems and technologies. *2018 IEEE Workshop on Complexity in Engineering (COMPENG)*, 1-6. Retrieved from https://api.semanticscholar.org/CorpusID:53436648

Bustamante, S., González, J., Lopez, G. J., & Cardona, H. A. (2023). Ufls and smart load for frequency regulation in electrical power system: A review. *IEEE Access*, *11*, 110967-

110984. Retrieved from https://api.semanticscholar.org/CorpusID:263684835

Cabrera-Tobar, A., Bullich-Massagué, E., Aragüés-Peñalba, M., & Gomis-Bellmunt, O. (2019). Active and reactive power control of a pv generator for grid code compliance. *Energies*, *12*(20). https://doi.org/10.3390/en12203872

Cerretti, A., Noce, C., Rochereau, H., & Schaupp, T. (2023). Requirements for generating plants to be connected in parallel with distribution networks - focus on en 50549 series. *IET Conference Proceedings*, *2023*, 681-685. https://doi.org/10.1049/icp.2023.0461

Chang, H., & Vanfretti, L. (2024). Power hardware-in-the-loop smart inverter testing with distributed energy resource management systems. *Electronics*. Retrieved from https://api.semanticscholar.org/CorpusID:271747336

Chmielowiec, K., Topolski, , Piszczek, A., & Hanzelka, Z. (2021). Photovoltaic inverter profiles in relation to the european network code nc rfg and the requirements of polish distribution system operators. *Energies*, *14*(5). https://doi.org/10.3390/en14051486

Chu, J., Yuan, L., Pan, H. N., & Hou, J. (2020). Primary frequency regulation requirement of south africa grid code and its digsilent simulation. *E3S Web of Conferences*. Retrieved from https://api.semanticscholar.org/CorpusID:219042103

Darbali-Zamora, R., Aparicio, M. J., Berg, J. C., & Gurule, N. S. (2026). Reinforcement-learning control for coordinated voltage regulation in distribution systems using a power hardware-in-the-loop platform. *IEEE Access*, *14*, 18298-18315. Retrieved from https://api.semanticscholar.org/CorpusID:285167246

Farooq, U., & Bass, R. B. (2022). Frequency event detection and mitigation in power systems: A systematic literature review. *IEEE Access*, *10*, 61494-61519. Retrieved from https://api.semanticscholar.org/CorpusID:249452360

Fortmann, J., Pfeiffer, R., Haesen, E., van Hulle, F., Martin, F., Urdal, H., & Wachtel, S. (2015). Fault-ride-through requirements for wind power plants in the entso-e network code on requirements for generators. *IET Renewable Power Generation*, *9*(1), 18-24. https://doi.org/https://doi.org/10.1049/iet-rpg.2014.0105

Gashi, A., Kabashi, G., Kabashi, S., Ahmetaj, S., & Veliu, V. (2012). Simulation of the wind grid code requirements for wind farms connection in

kosovo transmission grid. *Energy and Power Engineering*, *4*(6), 538–545. https://doi.org/10.4236/epe.2012.46062

Guise, L., Cleveland, F., Apostolov, A., Dawidczack, H., Berry, T., Schröder, A., & Otani, T. (2021, 11). *Facilitating the operation and integration of der and microgrids using the iec 61850-7-420 standard data models, especially for meeting ieee 1547 and en 50549 grid code requirements* (Vol. 2021).

Hafeez, Z. (2025). *Grid code compliance study of wind power plant using power system simulator for engineering (PSS/E)* (Master's thesis, Aalto University, Espoo, Finland). (Master's Thesis) Retrieved from https://urn.fi/URN:NBN:fi:aalto-202512159174

Hafezi, H., Laaksonen, H., Kauhaniemi, K., Lauttamus, P., & Strandberg, S. (2021). Power electronic converters simulation model verification for grid code compliance testing. In *2021 ieee pes innovative smart grid technologies europe (isgt europe)* (p. 01-06).

Hashimoto, J., Ustun, T. S., Suzuki, M., Sugahara, S., Hasegawa, M., & Otani, K. (2021). Advanced grid integration test platform for increased distributed renewable energy penetration in smart grids. *IEEE Access*, *9*, 34040-34053.

Hes, S., Kula, J., & Svec, J. (2019). Increasing der hosting capacity in lv grids in the czech republic in terms of european project interflex. *2019 IEEE PES Innovative Smart Grid Technologies Europe (ISGT-Europe)*, 1-5. Retrieved from https://api.semanticscholar.org/CorpusID:208210036

Heussen, K., Babazadeh, D., Degefa, M. Z., Taxt, H., Merino, J., Nguyen, V. H., ... Strasser, T. (2020). Test procedure and description for system testing. *European Guide to Power System Testing*. Retrieved from https://api.semanticscholar.org/CorpusID:226558501

International Energy Agency. (2026). *Total renewable capacity additions by technology, 2015–2025*. Paris: IEA. (Licence: CC BY 4.0) Retrieved from [2026-06-02]https://www.iea.org/data-and-statistics/charts/total-renewable-capacity-additions-by-technology-2015-2025

Jiménez, F., Gómez-Lázaro, E., Fuentes, J. A., Molina-García, A., & Vigueras-Rodríguez, A. (2012). Validation of a double fed induction generator wind turbine model and

wind farm verification following the spanish grid code. *Wind Energy*, *15*(4), 645-659. https://doi.org/https://doi.org/10.1002/we.498

Khan, M. K., Kauhaniemi, K., Laaksonen, H., & Hassan, M. A. (2026, January). Review of recent developments in grid codes: Focus on compliance testing and grid-forming inverter-based resources. *Renewable and Sustainable Energy Reviews*, *227*. https://doi.org/10.1016/j.rser.2025.116509

Khan, R., & Go, Y. I. (2019). Assessment of malaysia's large-scale solar projects: Power system analysis for solar pv grid integration. *Global Challenges*, *4*. Retrieved from https://api.semanticscholar.org/CorpusID:211077490

Kim, H., & Kim, J. (2024). Inertia-aware unit commitment and remuneration methods for decarbonized power system. *ArXiv*, *abs/2412.10820*. Retrieved from https://api.semanticscholar.org/CorpusID:274777334

Klaes, N. R., & Fortmann, J. (2025). Immunity of grid-forming control without energy storage to transient changes of grid frequency and phase. *IEEE Open Journal of the Industrial Electronics Society*, *6*, 265-276. Retrieved from https://api.semanticscholar.org/CorpusID:268259634

Krishnan, S. G., Aftab, M. A., Mohammed, N., Ahmed, S., & Konstantinou, C. (2025). Impact assessment of heterogeneous grid support functions in smart inverter deployments. *2025 IEEE PES Innovative Smart Grid Technologies Conference Europe (ISGT Europe)*, 1-5. Retrieved from https://api.semanticscholar.org/CorpusID:284358504

Kulkarni, N. G., & Virulkar, V. B. (2023, June). Enhancing the power quality of grid connected photovoltaic system during fault ride through: A comprehensive overview. *Journal of The Institution of Engineers (India): Series B*, *104*, 821–836. (Version of record published 30 March 2023; accepted 09 February 2023) https://doi.org/10.1007/s40031-023-00870-7

Kyesswa, M., Çakmak, H. K., Kühnapfel, U. G., & Hagenmeyer, V. (2020). Dynamic modelling and control for assessment of large-scale wind and solar integration in power systems. *IET Renewable Power Generation*. Retrieved from https://api.semanticscholar.org/CorpusID:226421320

Laine, H. (2020). *Grid code compliance testing using hil system* (Master's thesis, Tampere

University). Retrieved from https://trepo.tuni.fi/bitstream/handle/10024/120531/LaineHenri.pdf?sequence=2

Lee, H., Yoon, K.-H., Shin, J.-W., Kim, J.-C., & Cho, S.-M. (2020). Optimal parameters of volt–var function in smart inverters for improving system performance. *Energies*. Retrieved from https://api.semanticscholar.org/CorpusID:218954412

Lin, Y., Eto, J. H., Johnson, B. B., Flicker, J. D., Lasseter, R. H., Villegas Pico, H. N., … Yuan, G. (2022, March). Pathways to the next-generation power system with inverter-based resources: Challenges and recommendations. *IEEE Electrification Magazine*, *10*(1), 10–21. https://doi.org/10.1109/mele.2021.3139132

Liu, X., Xu, Z., & Wong, K. P. (2013). Recent advancement on technical requirements for grid integration of wind power. *Journal of Modern Power Systems and Clean Energy*, *1*, 216-222. Retrieved from https://api.semanticscholar.org/CorpusID:110297037

Marchgraber, J., & Gawlik, W. (2020). Dynamic voltage support of converters during grid faults in accordance with national grid code requirements. *Energies*, *13*, 2484. Retrieved from https://api.semanticscholar.org/CorpusID:219441342

Martínez-Lavín, M., Villena-Ruiz, R., Honrubia-Escribano, A., Hernández, J. C., & Gómez-Lázaro, E. (2022). Proposal for an aggregated solar pv power plant simulation model for grid code compliance. *Electric Power Systems Research*, *213*, 108676. https://doi.org/https://doi.org/10.1016/j.epsr.2022.108676

MathWorks. (2026). *Fmu export concepts*. MathWorks. (Accessed: June 7, 2026) Retrieved from https://se.mathworks.com/help/fmuexport/gs/fmuexport-concepts.html

Matiić, Z., Antić, T., Havelka, J., & Capuder, T. (2024). Voltage frequency differential protection algorithm. *Energies*. Retrieved from https://api.semanticscholar.org/CorpusID:269115724

Memon, A. A., Karimi, M., & Kauhaniemi, K. (2022). Evaluation of new grid codes for converter-based ders from the perspective of ac microgrid protection. *IEEE Access*, *10*, 127005-127030. Retrieved from https://api.semanticscholar.org/CorpusID:254217851

Misyris, G. S., Ramasubramanian, D., Mitra, P., & Singhvi, V. (2022). Locational aspect of fast frequency reserves in low-inertia systems - control performance analysis.

ArXiv, *abs/2207.08188*. Retrieved from https://api.semanticscholar.org/CorpusID:250626630

Moheb, A. M., El-Hay, E. A., & El-Fergany, A. A. (2022). Comprehensive review on fault ride-through requirements of renewable hybrid microgrids. *Energies*, *15*(18). https://doi.org/10.3390/en15186785

Muangchuen, S., Pahasa, J., & Ngamroo, I. (2023). Improved resilient model predictive control for enhanced microgrid virtual inertia emulation by virtual energy storage system under dos attacks. *IEEE Access*, *11*, 96817-96830. Retrieved from https://api.semanticscholar.org/CorpusID:261604612

Nanou, S. I., & Papathanassiou, S. A. (2014). Modeling of a pv system with grid code compatibility. *Electric Power Systems Research*, *116*, 301-310. https://doi.org/https://doi.org/10.1016/j.epsr.2014.06.021

Nomandela, S., Mnguni, M. E. S., & Raji, A. K. (2023). Modeling and simulation of a large-scale wind power plant considering grid code requirements. *Energies*, *16*(6). https://doi.org/10.3390/en16062897

Nomandela, S., Mnguni, M. E. S., & Raji, A. K. (2025). A case study on the validation of renewable energy grid code compliance for a large-scale wind power plant grid-connected mode of operation in real-time simulation. *Applied Sciences*, *15*(10). https://doi.org/10.3390/app15105521

Pahasa, J., Potejana, P., & Ngamroo, I. (2021). Multi-objective decentralized model predictive control for inverter air conditioner control of indoor temperature and frequency stabilization in microgrid. *Energies*. Retrieved from https://api.semanticscholar.org/CorpusID:239980704

Paturet, M., Markovic, U., Delikaraoglou, S., Vrettos, E., Aristidou, P., & Hug, G. (2019). Stochastic unit commitment in low-inertia grids. *IEEE Transactions on Power Systems*, *35*, 3448-3458. Retrieved from https://api.semanticscholar.org/CorpusID:102353678

Poudel, B., Guruwacharya, N., Subedi, S., Tamrakar, U., Wilches-Bernal, F., Rekabdarkolaee, H. M., … Tonkoski, R. (2024). Experimentation in exploring photovoltaic inverter dynamics under different irradiance levels through a data-driven approach. *IEEE Access*, *12*, 164137-164150. Retrieved from https://api.semanticscholar.org/

CorpusID:273738743

Sajadi, A., Kenyon, R. W., & Hodge, B.-M. S. (2021). Synchronization in electric power networks with inherent heterogeneity up to 100% inverter-based renewable generation. *Nature Communications*, *13*. Retrieved from https://api.semanticscholar.org/CorpusID:248525208

SFS-EN-50549-2:2019. (2019, February). *Requirements for generating plants to be connected in parallel with distribution networks – part 2: Connection to a mv distribution network – generating plants up to and including type b* (No. SFS-EN 50549-2:2019). Brussels, Belgium. (Published by CENELEC)

Shi, J., Cheng, Y., Zhang, F., Jiang, M., Lin, J., & Shen, Y. (2025, 08). *Gridcodex: A rag-driven ai framework for power grid code reasoning and compliance*.

Stanojev, O., Karaca, O., & Schweizer, M. (2025). Grid-forming vector current control frt modes under symmetrical and asymmetrical faults. *ArXiv*, *abs/2508.03389*. Retrieved from https://api.semanticscholar.org/CorpusID:280526767

Stojković, J., Lekić, A., & Stefanov, P. . (2020). Adaptive control of hvdc links for frequency stability enhancement in low-inertia systems. *Energies*. Retrieved from https://api.semanticscholar.org/CorpusID:229469120

Strasser, T. I., Andrén, F. P., Lauss, G., Bründlinger, R., Brunner, H., Moyo, C., ... Rodriguez-Seco, E. (2016). Towards holistic power distribution system validation and testing—an overview and discussion of different possibilities. *e & i Elektrotechnik und Informationstechnik*, *134*, 71 - 77. Retrieved from https://api.semanticscholar.org/CorpusID:254024241

Taul, M. G., Wang, X., Davari, P., & Blaabjerg, F. (2019). Current reference generation based on next-generation grid code requirements of grid-tied converters during asymmetrical faults. *IEEE Journal of Emerging and Selected Topics in Power Electronics*, *8*, 3784-3797. Retrieved from https://api.semanticscholar.org/CorpusID:201144173

Thiesen, H., & Jauch, C. (2021). Application of a new dispatch methodology to identify the influence of inertia supplying wind turbines on day-ahead market sales volumes. *Energies*. Retrieved from https://api.semanticscholar.org/CorpusID:233959951

Tuo, M., & Li, X. (2020). Dynamic estimation of power system inertia distribution us-

ing synchrophasor measurements. *2020 52nd North American Power Symposium (NAPS)*, 1-6. Retrieved from https://api.semanticscholar.org/CorpusID:219965634

Yıldırım, F., Doğan, E., Yalman, Y., Terciyanlı, E., Dindar, M., Kayar, E., … Çağatay Bayındır, K. (2026). A comprehensive comparative analysis of grid code requirements for renewable power plants and energy storage systems integration: Technical requirements, compliance assessments, and future directions for türkiye. *Electronics*. Retrieved from https://api.semanticscholar.org/CorpusID:286146316

Zeb, K., Islam, S. U., Khan, I., Uddin, W., Ishfaq, M., Curi Busarello, T. D., … Kim, H. (2022). Faults and fault ride through strategies for grid-connected photovoltaic system: A comprehensive review. *Renewable and Sustainable Energy Reviews*, *158*, 112125. https://doi.org/https://doi.org/10.1016/j.rser.2022.112125

Zenhom, Z. M., Aleem, S. H. E. A., Zahab, E. A., Ali, Z. M., Almalaq, A., & Boghdady, T. A. (2025). Synergistic hierarchical bi-level optimization of demand response programs and smart inverter volt/var control for maximizing hosting capacity of power systems with renewable-based distributed generators. *IEEE Access*, *13*, 15390-15409. Retrieved from https://api.semanticscholar.org/CorpusID:275703051

Appendices

Appendix 1. MATLAB Scripts for Compliance Curve Generation

```
%% EN 50549-2: UVRT Capability Plot

% Default Requirement (Solid Line)
% Points: (0;1) -> (0;0.05) -> (0.2;0.05) -> (2;0.85) -> (3;0.85)
t_def = [-0.5, 0, 0, 0.2, 2, 3, 3, 5];
U_def = [1.0, 1.0, 0.05, 0.05, 0.85, 0.85, 0.9, 0.9];

% --- 2. Plotting ---
figure('Color', 'w', 'Position', [100, 100, 850, 500]);
hold on;

% Plot Curves
plot(t_def, U_def, 'k-', 'LineWidth', 2, 'DisplayName', 'default
    requirement');
yline(0.9, 'b--', 'U = 0.9 pu', ...
      'LabelHorizontalAlignment', 'center', ...
      'FontSize', 10, 'LineWidth', 1.75);

% --- 3. Formatting and Grid ---
ax = gca;
set(ax, ...
    'Color', 'w', ...
    'XColor', 'k', 'YColor', 'k', ...
    'GridColor', 'k', ...
    'GridAlpha', 1, ...
    'FontWeight', 'bold')
grid(ax, 'on')
box on
ax.GridLineStyle = ':';
ax.GridColor = 'k';
ax.GridAlpha = 0.4;
ax.Layer = 'top';
```

```
32
33 % Labels and Limits
34 xlabel('Time [s]', 'FontSize', 12, 'FontWeight', 'bold');
35 ylabel('Voltage [p.u.]', 'FontSize', 12, 'FontWeight', 'bold');
36 xlim([-0.5, 4]);
37 ylim([0, 1.1]);
38 xticks(0:0.5:4);
39 yticks(0:0.2:1.2);
40
41 % --- 4. Annotating Key Points ---
42 text(0, 1.05, '(0;1)', 'FontSize', 9, ...
43      'HorizontalAlignment', 'center', 'Color', 'k');
44 text(-0.05, 0.08, '(0;0,05)', 'FontSize', 9, ...
45      'HorizontalAlignment', 'right', 'Color', 'k');
46 text(0.18, 0.02, '(0,2;0,05)', 'FontSize', 9, 'Color', 'k');
47 text(2, 0.88, '(2;0,85)', 'FontSize', 9, 'Color', 'k');
48 text(3, 0.83, '(3;0,85)', 'FontSize', 9, 'Color', 'k');
49 text(3, 0.93, '(3;0,9)', 'FontSize', 9, 'Color', 'k');
50
51 hold off;
```

Listing 1. MATLAB script for generating EN 50549-2 UVRT boundary curve.

```
1 %% EN 50549-2: OVRT Capability Plot
2
3
4 t = [-1, 0, 0, 0.1, 0.1, 2.1, 2.1, 3.1, 3.1, 5];
5 U = [1, 1, 1.25, 1.25, 1.20, 1.20, 1.15, 1.15, 1.10, 1.10];
6
7 % --- 2. Plotting ---
8 figure('Color', 'w', 'Position', [100, 100, 900, 500]);
9 hold on;
10
11 plot(t, U, 'k-', 'LineWidth', 2, 'DisplayName', 'default requirement');
12 yline(0.9, 'b--', 'U = 0.9 pu', ...
13       'LabelHorizontalAlignment', 'left', ...
14       'FontSize', 10, 'LineWidth', 1.75);
15 yline(1.1, 'b--', 'U = 1.1 pu', ...
```

```
      'LabelHorizontalAlignment', 'left', ...
      'FontSize', 10, 'LineWidth', 1.75);

% --- 3. Formatting and Grid ---
ax = gca;
set(ax, ...
    'Color', 'w', ...
    'XColor', 'k', 'YColor', 'k', ...
    'GridColor', 'k', ...
    'GridAlpha', 1, ...
    'FontWeight', 'bold')
grid(ax, 'on')
box on
ax.GridLineStyle = ':';
ax.GridColor = 'k';
ax.GridAlpha = 0.4;
ax.FontWeight = 'bold';

xlabel('Time [s]', 'FontSize', 12, 'FontWeight', 'bold');
ylabel('Voltage [p.u.]', 'FontSize', 12, 'FontWeight', 'bold');
xlim([-1, 5]);
ylim([0, 1.4]);

% --- 4. Adding Annotations ---
text(0, 0.93, '(0,0;1,0)', 'FontSize', 9, ...
     'HorizontalAlignment', 'center', 'Color', 'k');
text(-0.2, 1.28, '(0,0;1,25)', 'FontSize', 9, ...
     'HorizontalAlignment', 'center', 'Color', 'k');
text(0.1, 1.28, '(0,1;1,25)', 'FontSize', 9, ...
     'HorizontalAlignment', 'left', 'Color', 'k');
text(0.1, 1.17, '(0,1;1,20)', 'FontSize', 9, ...
     'HorizontalAlignment', 'left', 'Color', 'k');
text(2.1, 1.23, '(2,1;1,20)', 'FontSize', 9, ...
     'HorizontalAlignment', 'center', 'Color', 'k');
text(2.1, 1.12, '(2,1;1,15)', 'FontSize', 9, ...
     'HorizontalAlignment', 'center', 'Color', 'k');
text(3.1, 1.18, '(3,1;1,15)', 'FontSize', 9, ...
```

```
    'HorizontalAlignment', 'center', 'Color', 'k');
text(3.1, 1.07, '(3,1;1,10)', 'FontSize', 9, ...
    'HorizontalAlignment', 'center', 'Color', 'k');

hold off;
```

Listing 2. MATLAB script for generating EN 50549-2 OVRT boundary curve.

```
%% Q(U) Volt-Var Characteristic with Test Points

% --- 1. Parameters (Based on EN 50549-2 requirements) ---
V_nom = 100;         % Nominal Voltage (%)
Q_max = 33;          % Maximum Reactive Power (%)
slope = 5;           % Slope (%Q per %V)
V_low_start = 97;    % Deadband lower bound (%)
V_high_start = 103; % Deadband upper bound (%)

% --- 2. Calculate Saturation End Points ---
% dV_to_limit = Q_max / slope = 33/5 = 6.6% voltage deviation
dV_to_limit = Q_max / slope;
V_max_inj = V_low_start - dV_to_limit;  % +33% saturation point
V_max_abs = V_high_start + dV_to_limit; % -33% saturation point

% --- 3. Generate Theoretical Curve ---
V = linspace(80, 120, 500);
Q = zeros(size(V));

for i = 1:length(V)
    if V(i) < V_max_inj
        Q(i) = Q_max;                           % Max injection
    saturation
    elseif V(i) >= V_max_inj && V(i) < V_low_start
        Q(i) = (V_low_start - V(i)) * slope;    % Left linear slope
    elseif V(i) >= V_low_start && V(i) <= V_high_start
        Q(i) = 0;                               % Deadband
    elseif V(i) > V_high_start && V(i) <= V_max_abs
        Q(i) = (V_high_start - V(i)) * slope;  % Right linear slope
    else
```

```
        Q(i) = -Q_max;                          % Max absorption saturation
    end
end

% --- 4. Simulated Test Points (from compliance testing) ---
test_v = [80, 91, 93, 95, 98, 102, 105, 107, 108, 115];
test_q = [33, 30.31, 20.58, 11.1, 0, 0, -8.18, -19.17, -25.7, -32.7];

% --- 5. Plotting ---
fig = figure;
set(fig, 'Color', 'w');
hold on; grid on; box on;

% Theoretical curve
plot(V, Q, 'r', 'LineWidth', 2.5, ...
     'DisplayName', 'Q(U) Characteristic');

% Measured test points
plot(test_v, test_q, 'bo', 'MarkerFaceColor', 'g', ...
     'MarkerSize', 8, 'DisplayName', 'Test Points');

% Reference lines
line([100 100], [-40 40], 'Color', [0.5 0.5 0.5], ...
     'LineStyle', '--', 'HandleVisibility', 'off');
line([85 115], [0 0], 'Color', [0.5 0.5 0.5], ...
     'LineStyle', '--', 'HandleVisibility', 'off');

% Axis formatting
xlabel('Voltage V_{line} [%]', 'FontSize', 12, 'FontWeight', 'bold');
ylabel('Reactive Power Q [%]', 'FontSize', 12, 'FontWeight', 'bold');
title(['Q(U) Curve: Slope=5%, Dead-band=[', num2str(V_low_start), ...
       '%, ', num2str(V_high_start), '%]'], 'FontSize', 12);

ax = gca;
set(ax, 'XLim', [80, 120], 'YLim', [-40, 40], ...
        'Color', 'w', 'XColor', 'k', 'YColor', 'k', ...
```

```
        'GridColor', 'k', 'GridAlpha', 0.4, ...
        'FontWeight', 'bold');
grid(ax, 'on');
box on;

legend('Location', 'northeast');
hold off;
```

Listing 3. MATLAB script for generating Q(U) volt-var characteristic with test point validation.

```
%% LFSM-U Verification Plot (EN 50549-2) - Corrected X-Axis

% --- 1. Parameters ---
f_min = 47.5;       % Minimum frequency (Hz)
f1 = 49.8;          % Activation threshold frequency (Hz)
f_stop = 50.0;      % Nominal frequency (Hz)
s = 0.05;           % Droop coefficient (5%)
f_nom = 50;         % Nominal frequency (Hz)
tolerance = 10;     % +/- 10% Pn accuracy band

% --- 2. Create Frequency Vector (Left to Right: 47.5 to 50.0 Hz) ---
f = linspace(f_min, f_stop, 200);

% --- 3. Calculate Theoretical Droop Line (LFSM-U) ---
% Power is 0 at 50 Hz, stays 0 until 49.8 Hz, then increases
dP = zeros(size(f));
slope_indices = f < f1;
% Formula: dP = (f1 - f) / (s * f_nom) * 100
dP(slope_indices) = ((f1 - f(slope_indices)) ...
    ./ (s * f_nom)) * 100;

% --- 4. Calculate Tolerance Bounds ---
upper_band = dP + tolerance;
lower_band = dP - tolerance;

% --- 5. Plotting ---
fig = figure;
set(fig, 'Color', 'w', ...
```

```
          'Name', 'LFSM-U Standard Axis');
hold on; grid on;

% Shaded +/- 10% Pn Band
fill([f, fliplr(f)], [upper_band, fliplr(lower_band)], ...
     [0.7, 0.9, 1.0], 'EdgeColor', 'none', ...
     'FaceAlpha', 0.5, 'DisplayName', '\pm10\% Pn band');

% Theoretical Droop Curve
plot(f, dP, 'r', 'LineWidth', 2, ...
     'DisplayName', 'Theoretical (s=5\%)');

% --- 6. Simulated Test Points ---
test_freqs = [49.0, 49.2, 49.4, 49.6, 49.9];
test_dp = [31.95, 24.12, 16.1, 8.07, 0];

plot(test_freqs, test_dp, 'go', 'MarkerFaceColor', 'g', ...
     'MarkerSize', 8, 'DisplayName', 'Test points');

% --- 7. Formatting ---
xlabel('Frequency [Hz]', 'FontSize', 12, 'FontWeight', 'bold');
ylabel('\DeltaP/P_{ref} [\%]', 'FontSize', 12, 'FontWeight', 'bold');
title('LFSM-U Droop Curve (s=5\%, Deadband 49.8--50.0 Hz)', ...
      'FontSize', 12);

ax = gca;
set(ax, 'XLim', [47.5, 50.1], 'YLim', [-15, 85], ...
        'Color', 'w', 'XColor', 'k', 'YColor', 'k', ...
        'GridColor', 'k', 'GridAlpha', 0.4, ...
        'FontWeight', 'bold');
grid(ax, 'on');
box on;

legend('Location', 'northeast', 'Orientation', 'horizontal');
```

```
hold off;
```

Listing 4. MATLAB script for generating LFSM-U droop verification plot with tolerance band and test points.

```
%% LFSM-O Verification Plot (EN 50549-2) - Starts at 50 Hz

% --- 1. Parameters ---
f_start = 50.0;     % Start of plot (Hz)
f1 = 50.2;          % Activation threshold frequency (Hz)
f_max = 52.0;       % Maximum frequency (Hz)
s = 0.05;           % Droop coefficient (5%)
f_nom = 50;         % Nominal frequency (Hz)
tolerance = 10;     % +/- 10% Pn accuracy band

% --- 2. Create Frequency Vector ---
f = linspace(f_start, f_max, 200);

% --- 3. Calculate Theoretical Droop Line with Deadband ---
dP = zeros(size(f));
slope_indices = f > f1;
dP(slope_indices) = -((f(slope_indices) - f1) ...
    ./ (s * f_nom)) * 100;

% --- 4. Calculate Tolerance Bounds ---
upper_band = dP + tolerance;
lower_band = dP - tolerance;

% --- 5. Plotting ---
fig = figure;
set(fig, 'Color', 'w', ...
         'Name', 'LFSM-O Verification 50-52Hz');
hold on; grid on;

% Shaded +/- 10% Pn Band
fill([f, fliplr(f)], [upper_band, fliplr(lower_band)], ...
     [1, 0.9, 0.7], 'EdgeColor', 'none', ...
     'FaceAlpha', 0.5, 'DisplayName', '\pm10\% Pn band');
```

```
34
35 % Theoretical Droop Curve
36 plot(f, dP, 'r', 'LineWidth', 2, ...
37      'DisplayName', 'Theoretical (s=5\%)');
38
39 % --- 6. Simulated Test Points ---
40 test_freqs = [50.1, 50.4, 50.6, 50.8, 51];
41 test_dp = [0, -7.86, -15.83, -24, -31.58];
42
43 plot(test_freqs, test_dp, 'go', 'MarkerFaceColor', 'g', ...
44      'MarkerSize', 8, 'DisplayName', 'Test points');
45
46 % --- 7. Formatting ---
47 xlabel('Frequency [Hz]', 'FontSize', 12, 'FontWeight', 'bold');
48 ylabel('\DeltaP/P_{ref} [\%]', 'FontSize', 12, 'FontWeight', 'bold');
49 title('LFSM-O Droop Curve (Deadband 50.0--50.2 Hz, s=5\%)', ...
50       'FontSize', 12);
51
52 ax = gca;
53 set(ax, 'XLim', [50, 52], 'YLim', [-85, 15], ...
54         'Color', 'w', 'XColor', 'k', 'YColor', 'k', ...
55         'GridColor', 'k', 'GridAlpha', 0.4, ...
56         'FontWeight', 'bold');
57 grid(ax, 'on');
58 box on;
59
60 legend('Location', 'northeast', 'Orientation', 'horizontal');
61 hold off;
```

Listing 5. MATLAB script for generating LFSM-O droop verification plot with tolerance band and test points.

Appendix 2. Simulation Setup

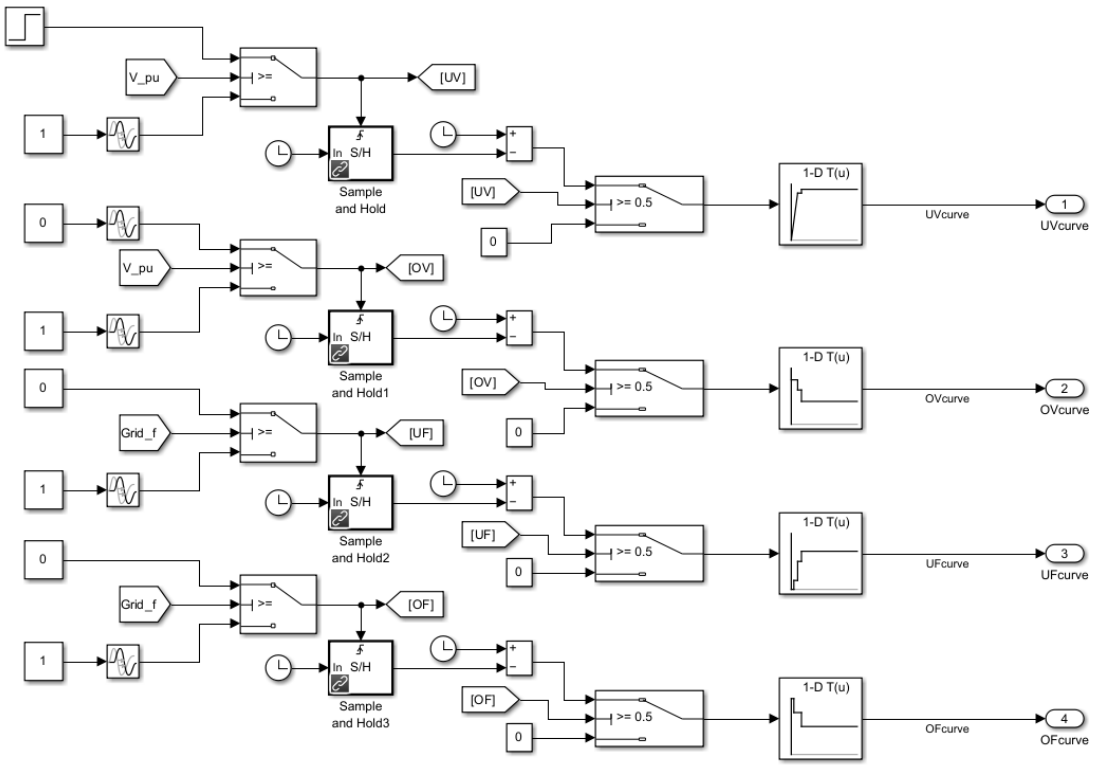

Figure 29. EN 50549-2 standard voltage and frequency ride-through boundary curves: UVRT, OVRT, UFRT, and OFRT capability used as reference for compliance testing.

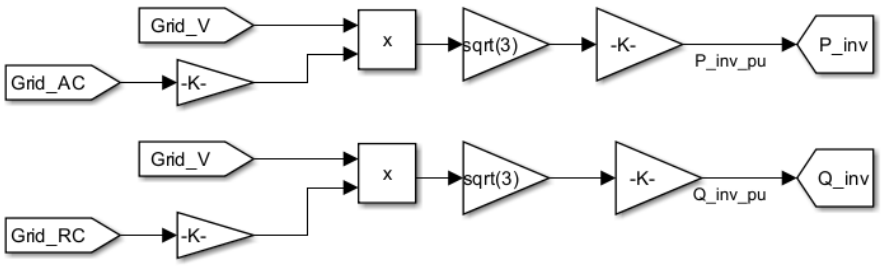

Figure 30. Simulation setup snapshot showing the active and reactive power calculation block configuration.

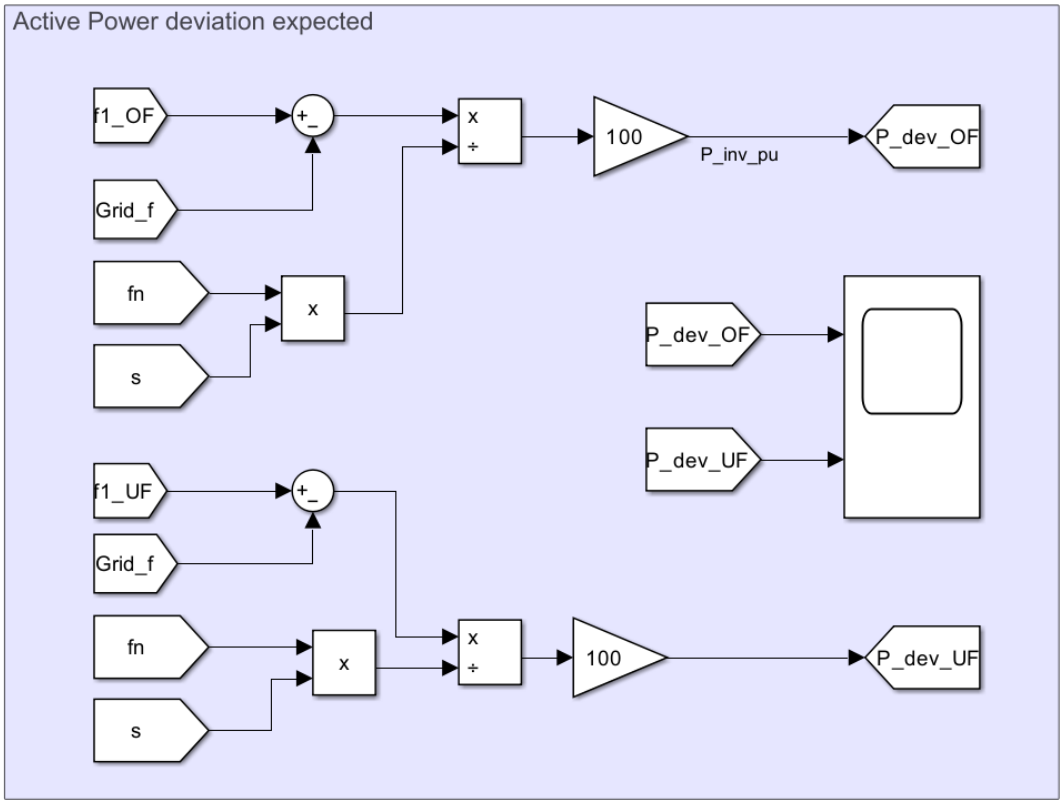

Figure 31. Simulation setup snapshot of the expected active power deviation reference signal generation.

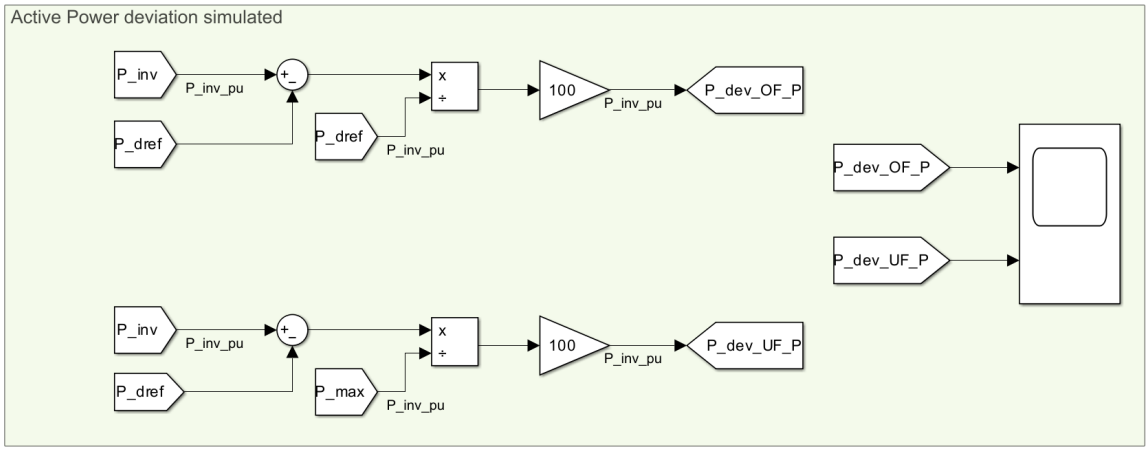

Figure 32. Simulation setup snapshot showing the simulated active power deviation measurement subsystem.

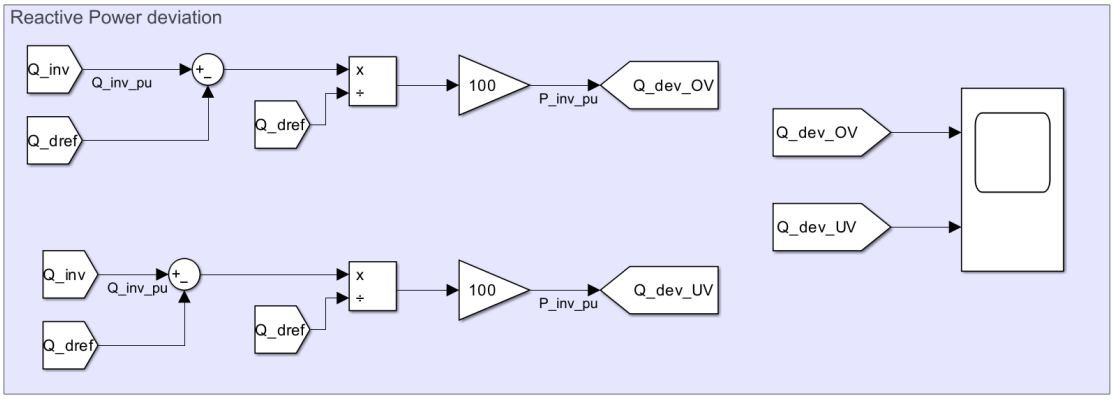

Figure 33. Simulation setup snapshot of the reactive power deviation monitoring and logging configuration.

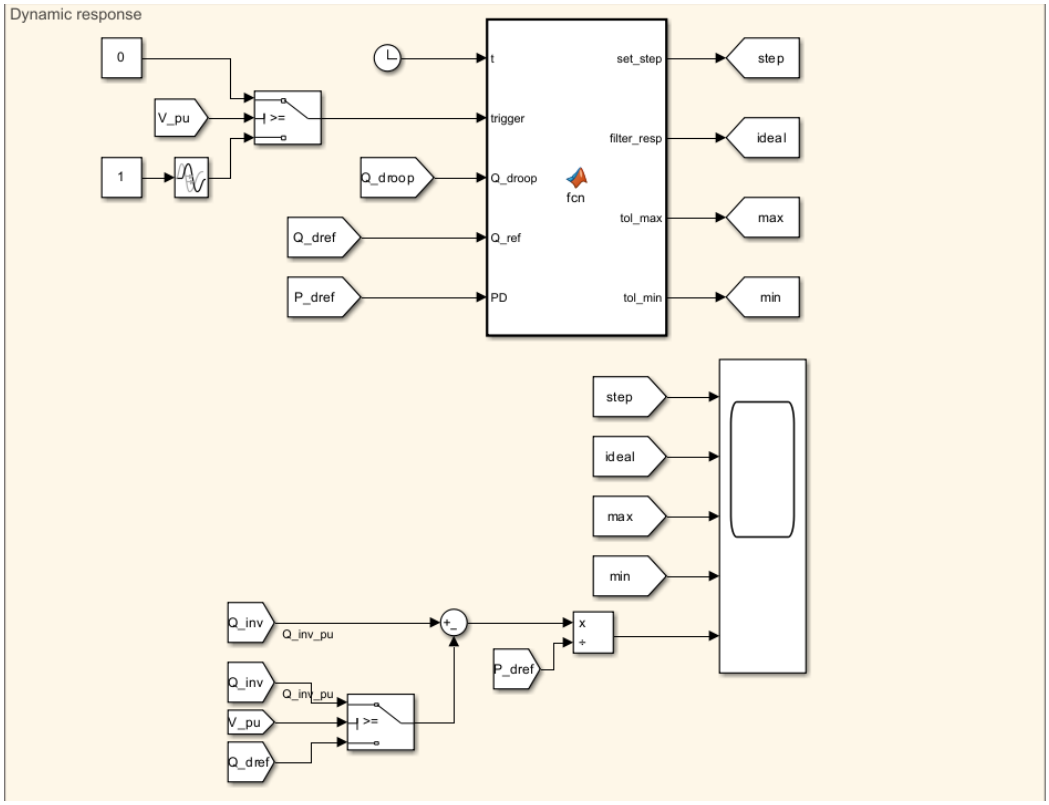

Figure 34. Simulation setup snapshot for the dynamic step response test of reactive power.